



Aspects of diffractive physics

Introduction of non-perturbative effects



RESEARCH REPORT PRESENTED IN PARTIAL FULFILLMENT OF
THE REQUIREMENTS FOR THE GRADE OF
DIPLOME D'ETUDE APPROFONDIES EN SCIENCES

Dechambre Alice

I would like to thank Jean-René Cudell for all his advices, his support and his attention during all this work. I would like also to underline his constant kindness and patience with me. I thank him for accepting me as a PhD student, I shall do my best. I also thank the group of fundamental theoretical physics, Joseph Cugnon and Lech Szymanowski for the discussions.

A special thanks to my sisters Amélie and Méline who studied all this time with me, to all my family and *maybe* to Vincent. I also think to Jean-Philippe, Max, Arthur, Cedric my officemate and Sophie for the help, coffee (or tea) breaks and all these discussions about anything. I finally warmly thank Arnaud for the original picture on the cover.

Contents

Introduction	4
1 Diffractive production in physics	5
1.1 Definition of diffraction	5
1.1.1 A QCD laboratory	7
1.2 Unsolved problems in diffractive QCD	8
1.3 Diffractive production of the Higgs boson	10
1.4 Plan of this work	11
2 Cutting rules for Feynman diagrams	13
2.1 Diagrams and dispersion relations	13
2.1.1 Branch-cut singularity	14
2.1.2 Dispersion relations	16
2.2 Cutting rules	18
2.3 Sudakov variables	19
2.3.1 Mathematical approach	19
2.4 A complete calculation of a one-loop diagram	22
2.4.1 Complete calculation	22
2.4.2 Cutting rules calculation	29
2.4.3 The REDUCE version	31
2.5 Conclusion	32
3 Diffractive pomeron physics	33
3.1 An introduction to the pomeron	33
3.2 Calculation organization	34
3.2.1 k_{\perp} factorization	34
3.2.2 Intermediate quarks	37
3.2.3 Method and physical interpretation	37
3.3 A simple impact factor	38
3.3.1 Imaginary part of the amplitude	45
3.4 Outlook	47
4 Non-perturbative effects: the Gribov conception	48
4.1 The gluon propagator	48
4.1.1 The Gribov idea	48
4.2 Contribution from the Gribov poles to the pomeron	50
4.2.1 Two-gluon exchange amplitude in the Gribov case	50
4.2.2 Properties of the new contribution	53
4.3 Conclusion and outlook	56

Conclusion	57
A Integration by residue	58
A.1 Residue theorem	58
B Feynman rules	60
B.1 Feynman rules for QCD	60
B.2 Feynman rules for ϕ^3 theory	61
C REDUCE programs	62
C.1 One loop diagram in Sudakov variables	63
C.2 Two gluon exchange	64
C.3 Gribov contribution	66
C.3.1 Symmetry property of diagram in the large s limit	68

Introduction

High-energy Quantum Chromodynamics (QCD) is now a topic at the center of the debate from the theoretical and experimental point of view, largely because of the opening of the Large Hadron Collider in 2007. This new large accelerator will have an energy in the center-of-mass system equal to $\sqrt{s} = 14$ TeV and is expected to be the scene of important events for physics.

Firstly, the energy available will allow the production of heavy particles such as the wanted Higgs boson or other exotic particles. Secondly, we could test high-energy theories such as supersymmetry or string theory but also simply check the reliability of our *good old* Standard Model for which the Higgs is a needed ingredient that must be found to confirm it. Theoretically, high-energy calculations lead to simplifications and relatively good predictions especially in the domain of hard interactions even if there are some details in the theory that have to be improved. High-energy physics is then a new, fascinating playing field for theorists and experimentalists alike.

Furthermore, high-energy calculations and particle production in QCD constitute a vast topic and, in this work we shall concentrate on one aspect, which we believe to be an interesting regime for particle production: diffractive physics and how it can lead to Higgs boson production. The second part of this work will use a different approach to QCD. One knows that perturbative theories are a really useful tools in QCD but unfortunately they are not sufficient to solve all the problems. Confinement, the structure of heavy particles and the gluon exchanges need more than perturbative calculations, i.e. the introduction of non-perturbative effects in order to describes the soft regime of interactions. Hence, the last chapter of this work will be a incursion into non-perturbative calculations.

We think of this work as a basis, a kind of manual or short report on topics, tools and methods for diffractive high-energy calculations and as an example of what is possible to do, but also as a bridge to new approaches to the introduction of non-perturbative effects and to more complex calculations.

Chapter 1

Diffractive production in physics

In a few words, diffraction is characterized by the production of particles without changing the quantum numbers of the colliding nucleons. Such a production is also characterized by a large rapidity gap between the produced hadrons and it was suggested by Bjorken [1] as a means of detecting new physics in hadron-hadron or hadron-lepton collisions. Diffractive scattering accounts for an important part of the total cross section of scattering processes and leads to a very clean detection of the products. This chapter is an introduction to the diffractive production of particles and to its use in the production of the Higgs boson.

In this chapter, we first define diffraction and explain its interests. In the second section, we discuss present problems with diffractive QCD predictions. At the end, we come to the topic on interest and discuss the implication of diffraction on Higgs production.

1.1 Definition of diffraction

Let us begin by a reminder of rapidity and of its role in hadronic scattering.

The rapidity y is defined by

$$y = \frac{1}{2} \log \frac{E + p_z}{E - p_z}, \quad (1.1)$$

where E and p_z are respectively the energy of the particle and the component of the momentum in the z -direction also called the longitudinal momentum. This is the natural relativistic velocity variable according to its transformation property under a boost along the real axis [2]. High-energy hadronic events usually lead to an approximately flat distribution of their final-state hadrons in rapidity but, in the case of diffractive processes, the products are very well separated as we draw in Fig. 1.1. This particularity has several interests that we discuss in the next section but before that we have to define diffraction.

Hadronic diffractive processes are reactions which takes place at high energy and in which the particles or the ensemble of particles scattered have the same quantum numbers as the incident particles [3]. This is possible only if the exchange has the quantum numbers of the vacuum. Here, the trajectory is called the pomeron and in practice, diffractive reactions are characterized by a large, non exponentially suppressed, rapidity gap in the final state as in Fig. 1.1.b . A substantial fraction of the total cross section is due to diffractive reactions and there are three different types of diffractive processes:

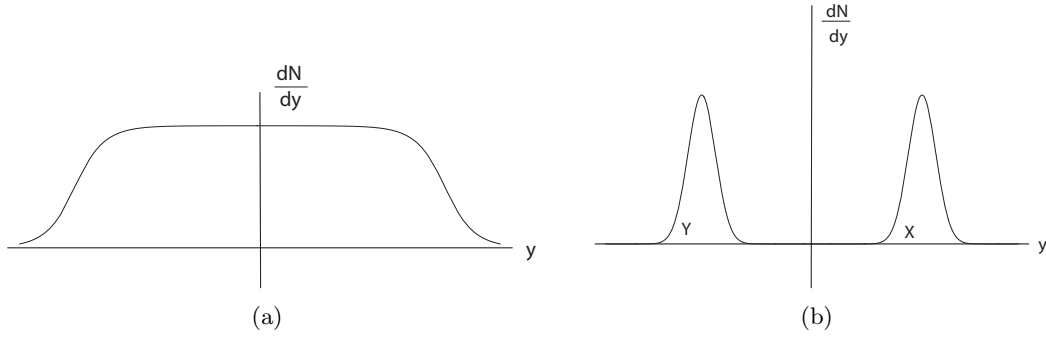


Figure 1.1: Distribution in rapidity dN/dy of the products of a central hadronic scattering (a) and a diffractive hadronic scattering (b).

1. **Elastic scattering:** Both incoming particles emerge intact in the final state with no loss of energy. See Fig. 1.2.a.
2. **Single diffractive scattering:** One of the incoming particle emerges almost unscathed with a small loss of energy. See Fig. 1.2.b.
3. **Double diffractive scattering:** Both of the incoming particles scattered and final particles have the same quantum number of the two initial particles. See Fig. 1.2.c.

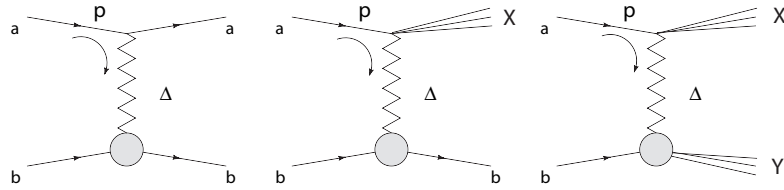


Figure 1.2: The three types of diffractive processes. The final states are well separated in rapidity and the zigzag lines denote the exchange of a trajectory with the vacuum quantum numbers.

For diffraction processes

$$M_{X,Y} \ll \sqrt{s_{ab}}, \quad (1.2)$$

the masses of the final states are much smaller than the energy in the center-of-momentum frame, s_{ab} . The essential variable is the fraction of momentum lost by the initial particle $x_{\mathcal{P}}$: if p is the four-momentum of the incoming proton then

$$\Delta \sim x_{\mathcal{P}} p, \quad (1.3)$$

The diffractive region is where $x_{\mathcal{P}}$ is small enough that pomeron exchange dominates¹ and this is the case for high-energy region.

¹As we explain in the next section, the pomeron trajectory and the exact nature of the pomeron are unsolved problems in QCD.

1.1.1 A QCD laboratory

Diffraction processes provide a QCD laboratory where we can investigate several aspects of QCD dynamics, soft and hard interactions, exotic particle production, non-perturbative effects or the high-energy behavior of the cross section. We will now come to the interest of the study of diffractive processes.

The first step of diffraction was the prediction of the behavior of the total cross section at high energy. This part was also tested in elastic hadron-hadron scattering where the behavior of the cross section at high energy is dominated by the exchange of the pomeron. It appears that we have to separate the soft regime of energy that cannot be described by perturbative QCD and the hard regime. The idea of hard diffraction, i.e. diffraction from models that include perturbative QCD, was born in 1984 from Donnachie and Landshoff [4] and was developed later by Ingelman and Schlein [5]. It was rapidly confirmed by the UA8 experiment at the CERN $p\bar{p}$ collider [6] that data were in relatively good agreement with predictions. Many aspects of diffraction when a hard scale is present are well understood in QCD and we can use perturbative techniques. The phenomenological description is interesting because hard diffraction QCD allows us to formulate the dynamics in terms of quarks and gluons and gives us the possibility from this basis to extend the problem to the non-perturbative region where soft-diffractive processes can occur. This is the difficult topic of semi-hard diffraction that tries to describe the change from hard scales to soft scales, i.e. from short-distance physics to long-distance physics. Up to now, hard-diffraction QCD is used in the description of Diffractive Deep Inelastic scattering (DDIS) processes via Generalized Parton Distribution (GPD). All these studies can be related to the structure of the proton and can help us understand how several partons can interact, scatter or produce heavy and exotic particles as the Higgs boson [7].

The main practical interest of diffractive production is the rapidity gap between the produced hadrons, a large separation of the products of the collision without hadronic remnants such that the rare particles that can be produced decay without background [8, 9]. The rapidity distribution of the new particles is necessarily between the two hadronic remnants and allows a very clean detection², as we show in Fig.1.3. Furthermore, color-singlet exchange between

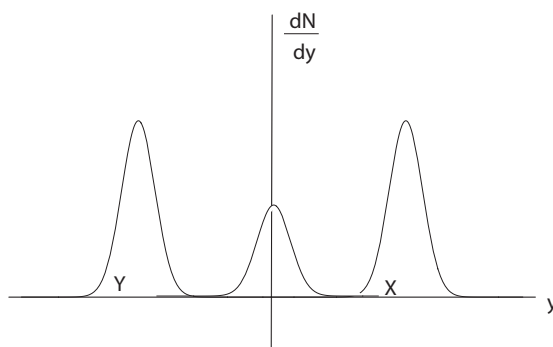


Figure 1.3: Distribution in rapidity of the products of a diffractive scattering.

protons is a very common event, about 25% of the cross section at the Tevatron³ is from elastic scattering $pp \rightarrow pp$ and another 20% is due to single-diffractive or double-diffractive

²In practice, this is only useful in the case of the decay products of the particles are easy to detect.

³From the Particle Data Group and [10].

scattering. Then, this aspect of QCD is important and will be even more so at the LHC because the center-of-momentum energy shall be equal to $\sqrt{s} = 14$ TeV. This energy will increase the rate of elastic scattering to about 30% of the total cross section [11] and may allow the production of heavy particles as the wanted Higgs bosons [12].

The surprise is that lowest-order QCD produces good estimates of diffractive processes even if there are many problems left such as the prediction of the form factor for pions or protons, the details in the infra-red region (IR) where we cannot apply perturbation theory, the nature of the pomeron, the implications of Regge theory or the introduction of longitudinal momentum transfer. This is the topic of the next section.

1.2 Unsolved problems in diffractive QCD

QCD has some problems to account for the details of diffraction. However, the relatively good agreement between lowest-order diffractive calculations and data leads us to believe that diffraction is an interesting challenge in the theory of strong processes, especially now with the LHC, where we shall have all the known diffractive processes but also new ones. Let us now look at three unsolved details in diffraction, the nature of the pomeron, the IR divergence and the BFKL prediction for the cross sections.

The nature of the pomeron

From Regge theory, a two-body scattering in the high-energy limit is described in terms of the exchange of Regge trajectories. Without going into too much detail, the amplitude is proportional to a power of the square energy, s

$$\mathcal{A} \propto s^{\alpha(t)}, \quad (1.4)$$

where t is the momentum transfer and $\alpha(t)$ is the *Regge trajectory*. A Taylor expansion of the trajectory in power series around $t = 0$ for t small enough gives

$$\alpha(t) = \alpha(0) + \alpha' t, \quad (1.5)$$

where $\alpha(0)$ is called the *intercept* and α' the *slope* of the trajectory. The total cross section behaves as a power of the intercept

$$\sigma_{tot} \sim \frac{1}{s} \text{Im}(\mathcal{A}(0)) \sim s^{\alpha(0)-1}. \quad (1.6)$$

As we have seen, diffractive production is based on the exchange of a trajectory with the quantum numbers of the vacuum called a pomeron. This pomeron is the dominant trajectory in elastic and diffractive high-energy processes and corresponds to the pomeron trajectory, fitted on data by Donnachie and Landshoff in [13]

$$\alpha_{\mathcal{P}}(t) = 1.08 + 0.25t, \quad (1.7)$$

and recently refitted to

$$\alpha_{\mathcal{P}}(t) = 1.09 + 0.3t, \quad (1.8)$$

in [14]. Unfortunately, QCD is useless to predict the value of $\alpha_{\mathcal{P}}(t)$. Besides, Regge poles correspond to bound states, i.e. exchanged particle that lie on the Regge trajectory and in

the case of the pomeron trajectory, such states called *glueballs* have not been observed yet⁴.

The difficulty with the pomeron and the QCD prediction of its trajectory is that even if we know that the pomeron makes the cross section rise at high energy, its exact nature is not well known. It could be a pole from the new Regge trajectory as we described previously and made of glueballs but also a BFKL pomeron as we explain in the next subsection or something else.

The IR region

Feynman rules for QCD define the usual gluon propagator in the Feynman gauge by

$$D_{\mu\nu}(k^2) = \frac{-i\delta^{ab}g_{\mu\nu}}{k^2 + i\epsilon}, \quad (1.9)$$

with k the four-momentum of the gluon and a, b the color indices. As we shall see in greater detail later, this propagator becomes huge at small momentum and is divergent at $k = 0$. Most of the time, we solve this problem via the introduction of an impact factor that removes the divergence and makes the cross section finite in the IR region. This impact factor is usually fitted to data or simulated by a quark dipole $q\bar{q}$.

One often supposes that the fact that the IR region is finite makes it small but it is not obvious. However, if it is not the case, we need to approximate the contribution from the IR region and to evaluate the uncertainties introduced.

The BFKL pomeron

Perturbative QCD calculations of the amplitude for high-energy processes are made through pomeron exchange [3]. The amplitude is the result of the sum of the leading $\log(s)$ contribution from the exchange of an infinite number of gluons between a pair of quarks, the BFKL pomeron. The summation procedure of all the $\log(s)$ contributions from each diagram is given by the BFKL equation developed by Balitsky, Fadin, Kuraev and Lipatov at the end of the seventies [16, 17].

The amplitude is the sum of the leading-log(s) contribution from gluon-exchange diagrams

$$\mathcal{A} \sim s \sum_n \alpha_s^2 (\alpha_s \log(s))^n, \quad (1.10)$$

where $(\alpha_s \log(s))^n$ is the leading $\log(s)$ contribution from the exchange of $n+2$ gluon between the quarks in the singlet mode. After BFKL resummation, the total cross section behaves as

$$\sigma \sim s^\omega \quad (1.11)$$

with ω the BFKL pomeron intercept in the leading order (LO)

$$\omega_{LO} \sim 12 \frac{\alpha_s}{\pi} \log(2). \quad (1.12)$$

The equation has the particularity to include all transverse momenta from soft contributions to hard ones so that all the scales are mixed. The prediction of BFKL for a value of α_s close to 0.2 is too large and leads to a cross section behavior as $\sim s^{0.53}$, far away from the data.

⁴Glueball are expected to be the bound states of at least two gluons, there is now a 2^{++} candidate and the reader can find more details about it in reference [15].

Nevertheless, the BFKL approach may reproduce the data only if we include huge non-leading corrections [18]. Another problem is that calculations are very sensitive to the details of the IR region where we have to include non-perturbative corrections that complicate the solution [6].

1.3 Diffractive production of the Higgs boson

A very interesting issue for diffractive physics is Higgs diffractive production. This idea was developed 10 years ago and is now ready to be tested in the new Large Hadron Collider. Actually, diffractive production is a potential Higgs discovery channel and lead to a lot of theoretical⁵ and experimental studies.

Higgs diffractive production is the process $pp \rightarrow pHp$ and an example of a possible kinematics is shown in Fig. 3.1. Most of the mechanisms of diffractive Higgs production are similar to

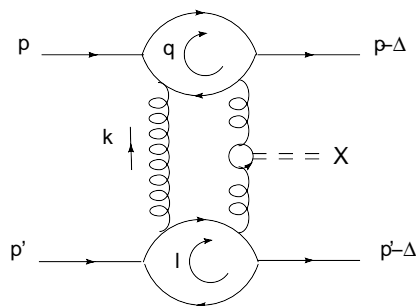


Figure 1.4: An example of diagram related to the diffractive cross section for the production of a Higgs boson in the high-energy limit.

this one inspired by the original paper of Bialas and Landshoff [20]. This mode of production is interesting because from the LEP results [21], the mass of the Standard Model Higgs boson is below 120 GeV. In this case, the largest decay branching ratio is

$$H^0 \rightarrow b\bar{b} \quad (1.13)$$

and the detection of a bottom pair is quasi impossible if a lot of hadrons are present in the detector. Hence, diffractive processes become very competitive because the momenta of the two final protons may be measured very accurately and this leads to a very clear estimate of the Higgs mass with missing mass technique [22]. Furthermore, the background⁶ is flat and we can well separate it from the Higgs resonance peak. Another advantage will be the huge energy available at the LHC that will increase the cross section of such a production. First of all, the energy available will increase the elastic part of the cross section and then increase the number of diffractive events. A lot of studies of the cross section for diffractive Higgs production have been made and lead to estimates that differ by several orders of magnitude [8, 23]. In the table 1.1, we summarize the predicted cross section based upon recent QCD calculations for diffractive production of a Higgs boson of mass about 120 GeV at LHC energies, the last column gives the expected number of events for the first year of running. If we think that 100 events are necessary to lead to the detection of the Higgs boson

⁵See [19] for a recent theoretical study.

⁶The background is composed of b and \bar{b} quarks that don't come from Higgs decays.

Reference	Process	σ_{Higgs} (fb)	Number of events First year
<i>Cudell and Hernandez</i> [8]	quasielastic	300	9000
	double diffractive	1200	36000
<i>Durham group</i> [24]	quasielastic	3	90
	double diffractive	40	1200
<i>Enberg, Ingelman, Kissavos Timneanu</i> [25]	double diffractive	0.2	6

Table 1.1: Recent QCD calculations of the cross section for quasielastic and double diffractive production of a Higgs boson of mass about 120 GeV at the LHC energy, from [26]. The number of events the first year of running is calculated for an integrated luminosity equal to 30 fb^{-1} .

then it can be discovered the first year of running or in 16 years according to the last reference.

However, this production is not the topic of this work, that serves as an introduction to the tools needed to calculate this process and then the reader should consider Higgs production as the continuation of the present work.

1.4 Plan of this work

We now have the necessary ingredients to understand diffractive production. We defined diffraction, its interest and the problems with diffractive QCD predictions. Our ultimate goal is diffractive Higgs production and to build a model that can correspond to data. We will present here our first steps in this direction.

The first chapter is an introduction to cutting rules. Diffractive cross sections in QCD calculations are made from Feynman diagrams and we shall see that the main part of the cross-section information is given by the imaginary part of the diagrams. Most of the time, this imaginary part is easier to compute than the total amplitude hence, we shall develop and remind the reader of techniques that relate the imaginary part to the total cross section. Firstly, we shall speak about the use of diagrams, dispersion relations and how to use them to find the total cross section of a scattering event. The second section introduces cutting rules, a powerful tool in order to calculate directly the imaginary part of a diagram and goes to the definition of Sudakov variables that we shall use in all this work. At the end of this chapter, we shall make a complete calculation of a simple process in order to illustrate and show the validity of all the tools introduced previously.

After the introduction of our technique of calculation we come to pomeron physics in the next chapter. As we show in the introduction, the pomeron is a main but not well-know ingredient in high-energy physics. Hence, we shall remind the reader of the definition of the pomeron and of its importance in our calculation. We shall also introduce the approach of our future calculations. Actually, the diffractive Higgs production diagrams can be separated

in different pieces that we can complicate separately in order to improve the calculation and to remove uncertainties. The last subsection is devoted to the first step in this direction, a two-loop diagram as a basis of our future works.

The last chapter will contain a original result. We know that QCD has some problems especially with non-perturbative phenomena, i.e. long-distance events. The introduction of non-perturbative effects in the calculation is very interesting because that leads to new questions in physics. A long time ago, Gribov introduced the idea of a modified gluon propagator that includes non-perturbative effects in the usual calculation of the amplitude. Then, we shall take this *Gribov propagator* and perform the calculation of two-gluon exchange with it. We shall present the calculation itself and make a brief discussion on the results. We conclude by a review of the improvements needed in the calculation and of the new aspects of the amplitude.

This work is then the first step to diffractive exotic particles production. We hope that it can be used as a kind of manual for diffractive calculations and a tool to more complex calculations.

Chapter 2

Cutting rules for Feynman diagrams

In particles physics, one of the experimental methods involves scattering of particles in accelerators. These collisions can be studied and lead to the most commonly calculated quantities in quantum field theory, the scattering cross sections. The total cross section, σ_t , is proportional to the probability of scattering to occur and comes from the probability of interaction of particles. This is a quantity that theorists compute and experimentalists can measure.

In order to calculate the cross section, we have a lot of useful tools, the most important ones being Feynman diagrams and more precisely the imaginary part of Feynman diagrams. In the present chapter, we are going to introduce those tools and we shall show how they can be used. Firstly, we briefly speak about diagrams, the optical theorem and dispersion relations, secondly we introduce cutting rules as a powerful tool to calculate directly the imaginary part of a Feynman diagram. The third section is a complete calculation of a simple process in QCD.

2.1 Diagrams and dispersion relations

First, let us remind the reader of notions such as the cross section, Feynman diagrams and the amplitude.

It is conventional to write the differential cross section for a $2 \rightarrow 2$ scattering process¹ as

$$\frac{d\sigma}{d\Omega} = \frac{1}{64\pi^2 E_{cm}^2} |\mathcal{M}|^2, \quad (2.1)$$

where $d\Omega$ is the solid angle in the center-of-momentum frame in which the final particles are produced [27]. The quantity \mathcal{M} is dimensionless, Lorentz invariant and known as the quantum-mechanical amplitude for the process to occur or the invariant amplitude. It is analogous to the scattering amplitude f in quantum mechanics and we can see that the physics resides in this amplitude. Most of the time, this amplitude can't be calculated exactly, even in very simple problems like QED processes but in order to evaluate it, we can use Feynman diagrams. Each scattering process can be represented with lines and vertices and translated directly into a contribution to \mathcal{M} by associating multiplicative factors with each elements of the diagram, this is the *Feynman rules*.

$$i\mathcal{M} = \Sigma(\text{all distinct and connected Feynman diagram for the process}).$$

¹As an example, the annihilation reaction $e^+e^- \rightarrow \mu^+\mu^-$.

Some of these rules [28] are given in Appendix B. Usually, this contribution is real and leads to a real amplitude for the process but if there are poles in the propagators, the amplitude has an imaginary part. Some Feynman diagrams have an imaginary part and let us discuss the interest of this part.

The total amplitude for a process is the sum of the associated Feynman diagrams and these diagrams lead to a purely real amplitude unless some denominators vanish and, in this case, the diagrams have a non-zero imaginary part that contributes to the amplitude. Physically, this happens when the virtual intermediate-state particles in the diagram go on-shell. We show in Fig. 2.1 two examples of diagrams, the first has an intermediate state that can be on-shell and leads to an imaginary part of the amplitude, the second is purely real. The amplitude

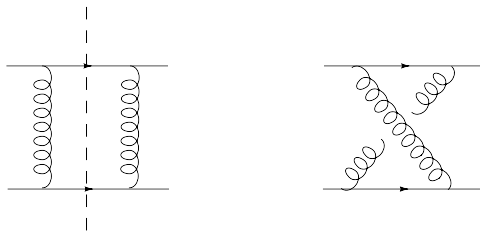


Figure 2.1: Example of diagrams, the first leads to an imaginary contribution to the amplitude, the second is purely real.

for a process is the sum of all possible diagrams and hence, we have to calculate both the imaginary part and the real part. However, we can make our work easier by considering at the start, only the imaginary part of the amplitude. The advantages are that

1. for a given process, there are fewer diagrams leading to an imaginary contribution than diagrams contributing to the real part;
2. these diagrams can be easily evaluated with the help of cutting rules as we explain in the next section;
3. we can often obtain the real part of the amplitude via dispersion relation.

Because of this, we prefer computing the imaginary part of the amplitude and construct the real part from it.

Let us now study the quantity \mathcal{M} defined by the Feynman rules in perturbation theory.

2.1.1 Branch-cut singularity

The definition of \mathcal{M} in the formalism allows us to consider it as a function of the energy in the center-of-momentum frame, E_{cm} . First, we shall introduce some useful quantities, the Mandelstam variables, after that, we shall speak about the analytic structure of \mathcal{M} as a function of the energy.

We define the Mandelstam variables and consider a system with two initial particles with four-momenta p_1 and p_2 as shown in Fig. 2.2. This notation will be our usual notation for

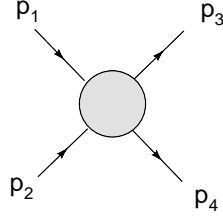


Figure 2.2: Label of the four external momenta.

incoming and outgoing particles and we have

$$s = (p_1 + p_2)^2 = (p_3 + p_4)^2, \quad (2.2)$$

$$t = (p_1 - p_3)^2 = (p_2 - p_4)^2, \quad (2.3)$$

$$u = (p_1 - p_4)^2 = (p_2 - p_3)^2. \quad (2.4)$$

In these variables, s is the square of the energy in the center-of-momentum $s = E_{cm}^2$ and t the square of the four-momentum transfer.

According to Feynman rules in perturbation theory, we can consider \mathcal{M} as an analytic function of the complex variable s and we define $\sqrt{s_0}$ as the threshold energy for production of the lightest multiparticle state. If the energy in the center-of-momentum frame is smaller than $\sqrt{s_0}$, the intermediate states cannot go on-shell, there are no poles on the real axis and no contribution to the imaginary part of the amplitude: $\mathcal{M}(s)$ is real. Because of that, we have the identity

$$\mathcal{M}(s) = [\mathcal{M}(s^*)]^*, \quad (2.5)$$

each side of the equation is an analytic function of s , then $\mathcal{M}(s)$ can be analytically continued to the entire complex s plane. Near the real axis, i.e. at $s \pm i\epsilon$ with s and ϵ real, eq. (2.5) implies

$$\mathcal{M} = \text{Re}\mathcal{M}(s + i\epsilon) = \text{Re}\mathcal{M}(s - i\epsilon). \quad (2.6)$$

There is no discontinuity for $s < s_0$ because there is no imaginary part. However, for $s > s_0$, there is enough energy to allow on-shell intermediate states which lead to branch cuts on the real axis. The analytic function $\mathcal{M}(s)$ is such as

$$\text{Re}\mathcal{M}(s + i\epsilon) = \text{Re}\mathcal{M}(s - i\epsilon), \quad (2.7)$$

$$\text{Im}\mathcal{M}(s + i\epsilon) = -\text{Im}\mathcal{M}(s - i\epsilon). \quad (2.8)$$

The imaginary part becomes non zero and its sign changes when we cross the real axis, this is the *discontinuity across the real axis* starting at the threshold energy s_0 . The discontinuity across the cut, i.e. at the singularity, is

$$\text{Disc}\mathcal{M}(s) = 2i\text{Im}\mathcal{M}(s + i\epsilon). \quad (2.9)$$

This relation is easy to check for a one loop diagram and it is done in [27].

Optical theorem for Feynman diagrams

Before closing this section, let us say a few words about the optical theorem in high-energy physics. It can be used to related the imaginary part of $\mathcal{M}(s)$ to the total scattering cross section, a measurable quantity.

The optical theorem is a straightforward consequence of the unitary of the S -matrix and it says that the imaginary part of a forward scattering amplitude at $t = 0$ is proportional to the total cross section. The standard form of the optical theorem in reference [27] is

$$\text{Im}\mathcal{M}(p_1, p_2 \rightarrow p_1, p_2)_{t=0} = 2E_{cm}p_{cm}\sigma_{tot}(p_1, p_2 \rightarrow \text{anything}), \quad (2.10)$$

where E_{cm} is the total center-of-momentum energy and p_{cm} is the momentum of either particle in the center-of-momentum frame. This arises from a sum of contributions from all possible intermediate-state particles as we show graphically in Fig. 2.3. We have now a re-

Figure 2.3: A graphical representation of the optical theorem with the sum of contributions from all possible intermediate-state particles Π_f .

lation between the amplitude that can be calculated from Feynman diagram and the total cross section.

2.1.2 Dispersion relations

Dispersion relations² allow the computation of the complete scattering amplitude from the knowledge of its imaginary part. The method was inspired by the Kramers-Krönig relations in optics for the index of refraction of a medium [29]. These relations express the real part of the amplitude for forward scattering at a fixed squared energy s as an integral of the imaginary part of the amplitude (absorptive part) over all square energy s' . The dispersion relations come from the fact that the function $\mathcal{M}(s)$ is analytic and from the use of Cauchy's theorem³ to relate the imaginary and real part of $\mathcal{M}(s)$ on the real axis [30].

Let us consider the function $\mathcal{M}(s)$ analytic in the upper half s plane. For any point s inside a closed contour C as we draw in Fig. 2.4 Cauchy's theorem gives

$$\mathcal{M}(s) = \frac{1}{2i\pi} \oint_C \frac{\mathcal{M}(s')}{s' - s} ds', \quad (2.11)$$

with

$$\oint_C \frac{\mathcal{M}(s')}{s' - s} ds' = \int_{-\infty}^{\infty} \frac{\mathcal{M}(s')}{s' - s} ds' + \int_{C_\infty} \frac{\mathcal{M}(s')}{s' - s} ds' + \int_{C_\epsilon} \frac{\mathcal{M}(s')}{s' - s} ds'. \quad (2.12)$$

²Dispersion relations are used and well known in optics where they are usually called Kramers-Krönig relations.

³Theorem of integration along a closed curve given Appendix A.

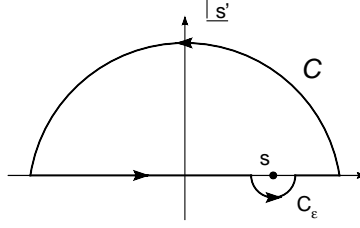


Figure 2.4: Integration contour in the case of the dispersion relations.

Generally for high-energy processes the function $\mathcal{M}(s')$ vanishes sufficiently rapidly at infinity so that there is no contribution to the integral from the half semicircle contour [31], hence

$$\mathcal{M}(s) = \frac{1}{2i\pi} \left[\int_{-\infty}^{\infty} \frac{\mathcal{M}(s')}{s' - s} ds' + \int_{C_\epsilon} \frac{\mathcal{M}(s')}{s' - s} ds' \right]. \quad (2.13)$$

If the pole s is now any point in the upper half plane and if we take the limit as the complex energy approaches the real axis from above, we write $s = s + i\epsilon$ with ϵ very small and

$$\mathcal{M}(s + i\epsilon) = \frac{1}{2i\pi} \left[\int_{-\infty}^{\infty} \frac{\mathcal{M}(s')}{s' - s - i\epsilon} ds' + \int_{C_\epsilon} \frac{\mathcal{M}(s')}{s' - s - i\epsilon} ds' \right]. \quad (2.14)$$

If $\epsilon \rightarrow 0$,

$$\begin{aligned} \mathcal{M}(s) &= \lim_{\epsilon \rightarrow 0} \mathcal{M}(s + i\epsilon) \\ &= \frac{1}{2i\pi} \left[\text{P} \int_{-\infty}^{\infty} \frac{\mathcal{M}(s')}{s' - s} ds' + i\pi \mathcal{M}(s) \right], \end{aligned} \quad (2.15)$$

which leads to

$$\mathcal{M}(s) = \frac{i}{\pi} \text{P} \int_{-\infty}^{\infty} \frac{\mathcal{M}(s')}{s' - s} ds'. \quad (2.16)$$

where P denotes the principal part of the integral. The real part and the imaginary part of the last equation are

$$\text{Re}\mathcal{M}(s) = \frac{1}{\pi} \text{P} \int_{-\infty}^{\infty} \frac{\text{Im}\mathcal{M}(s')}{s' - s} ds', \quad (2.17)$$

$$\text{Im}\mathcal{M}(s) = -\frac{1}{\pi} \text{P} \int_{-\infty}^{\infty} \frac{\text{Re}\mathcal{M}(s')}{s' - s} ds'. \quad (2.18)$$

The sign behind the two parts depends on the half s plane where the function is analytic. If the contribution from the half semicircle C_∞ doesn't vanish, eq. (2.15) becomes

$$\mathcal{M}(s) = \frac{i}{\pi} \text{P} \int_{-\infty}^{\infty} \frac{\mathcal{M}(s')}{s' - s - i\epsilon} ds' + C_\infty. \quad (2.19)$$

This term may be suppressed by making a subtraction, this means considering the amplitude $\mathcal{M}(s)/s$ instead of $\mathcal{M}(s)$: it has an extra-pole in $s = 0$ but a better behavior at infinity. For instance, if the amplitude is constant at $s \rightarrow \infty$ the dispersion relations are given by

$$\frac{\text{Re}\mathcal{M}(s)}{s} = \frac{\text{Re}\mathcal{M}(0)}{s} + \frac{1}{\pi} \text{P} \int_{-\infty}^{\infty} \frac{\text{Im}\mathcal{M}(s')}{s'(s' - s)} ds', \quad (2.20)$$

which is called a dispersion relation with one subtraction.

Then, we have expressed the real part of a forward-scattering amplitude \mathcal{M} in terms of a dispersion relations over its imaginary part.

2.2 Cutting rules

In the present section, we will introduce a powerful tool to compute directly the imaginary part of a Feynman diagram: the *Cutkosky rules* or cutting rules proven by Cutkosky in 1960 [32]. Discontinuities of a diagram give precisely twice the imaginary part that we need to obtain the total cross section with the help of the optical theorem. Cutkosky showed that the physical discontinuity of any multiloop Feynman diagram is given by a set of simple rules⁴, the cutting rules.

In the region of momentum integration for a given Feynman diagram, every time that one or more propagators can simultaneously go on-shell, the value of the discontinuity is given by the substitution of each of the two propagators with a delta function

$$\frac{1}{p_i^2 - m^2 + i\epsilon} \rightarrow -2i\pi\delta_+(p_i^2 - m^2). \quad (2.21)$$

Note the δ_+

$$\delta_+(p_i^2 - m^2) = \delta(p_i^2 - m^2)\theta(p_i^0), \quad (2.22)$$

because each cut corresponds to a particle so that energy must be positive and there are some constraints on the integration. Poles of the additional propagators do not contribute and we show an example of a cut diagram in Fig. 2.5. So, to compute the discontinuity of a

$$2\text{Im} \left[\text{Diagram with cut} \right] = \int d\Pi \left| \text{Diagram with cut} \right|^2$$

Figure 2.5: An example of a cut diagram and the contribution to the imaginary part of the amplitude.

Feynman diagram, we use the following method:

1. Cut through the diagram in all possible ways such that the cut propagators can simultaneously be put on-shell.
2. For each cut, replace the propagators using eq. (2.21), then perform the loop integrals.
3. Sum the contribution of all possible cuts.

From the discontinuity, we can find the imaginary part of the amplitude via eq. (2.9).

Now, we better understand the structure of our next calculations and the interest of the imaginary part of the amplitude. Our method shall be: compute the imaginary part of some Feynman diagrams by cutting rules and use dispersion relations to find the real part. The imaginary part can be used too in order to obtain the total cross section of processes from the

⁴These rules are simple only for singularities in the physical region.

optical theorem. Thus far, we gave the method of cutting. Usually, it is easier to compute the discontinuity of a diagram with the help of cutting rules than to calculate the imaginary part directly and we shall often use this powerful tool.

2.3 Sudakov variables

Now, as we have introduced our tools for the amplitude calculations, we present our variables. During the rest of this work, we will use some useful variables called *Sudakov variables* of a given four-vector.

Physical approach

Let us first consider an intuitive approach. The Sudakov representation is a decomposition of the intermediate state four-momenta q upon the incoming particles four-momenta, p_1 and p_2 . So, we have three privileged directions, the directions of the ingoing particles plus the transverse direction. With this particular decomposition,

$$q = \alpha p_1 + \beta p_2 + q_\perp, \quad (2.23)$$

we can immediately see that α is the part of the four-momentum in the p_1 direction, β the part in the p_2 direction and q_\perp the part of the momenta in the perpendicular direction. A small β indicates that the intermediate particles are more in the direction of the ingoing particles p_1 than in the p_2 direction. In addition to these advantages, we have the covariance of q , i.e. a Lorentz transform changes the four-vectors p_1 and p_2 simply and keeps α and β unchanged. We have two invariants that lead to the physical interpretation of the variables and this will give us a good intuition for what happens during a scattering process.

2.3.1 Mathematical approach

From the mathematical point of view, let us consider a system with two initial particles with four-momenta p_1 and p_2 as shown in Fig. 2.6. We work with non-vanishing masses M for the

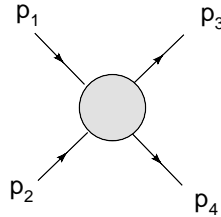


Figure 2.6: Label of the four external momenta.

initial particles,

$$p_1 \cdot p_1 = M^2, \quad (2.24)$$

$$p_2 \cdot p_2 = M^2, \quad (2.25)$$

and use Mandelstam variables. It is immediate from the definition in eq. (2.3) that

$$\begin{aligned}
s &= p_1^2 + p_2^2 + 2p_1 \cdot p_2, \\
&= 2M^2 + 2p_1 \cdot p_2 \quad \rightarrow \quad p_1 \cdot p_2 = \frac{s - 2M^2}{2}.
\end{aligned} \tag{2.26}$$

In the high-energy limit, $s \gg M^2$ then

$$p_1 \cdot p_2 \sim \frac{s}{2}. \tag{2.27}$$

This is the relation that we will use in the rest of this work. We now come back to eq. (2.23). The transverse momentum q_\perp is a transverse vector, i.e.

$$\begin{aligned}
q_\perp \cdot p_1 &= 0, \\
q_\perp \cdot p_2 &= 0.
\end{aligned} \tag{2.28}$$

Hence we have the change of variable

$$(q_0, q_x, q_y, q_z) \rightarrow (\alpha, \beta, \vec{q}_\perp), \tag{2.29}$$

where \vec{q}_\perp has two degrees of freedom. We have to calculate the associated jacobian. In the center-of-momentum frame, it is possible to choose the z -axis such that

$$p_1 = \left(\frac{\sqrt{s}}{2}, 0, 0, \frac{\sqrt{s}}{2} \right), \tag{2.30}$$

$$p_2 = \left(\frac{\sqrt{s}}{2}, 0, 0, -\frac{\sqrt{s}}{2} \right). \tag{2.31}$$

This means that the ingoing particles move along the z -axis coming from opposite directions⁵. We can write the matrix of the change of variables for the first and fourth variables,

$$\begin{pmatrix} q_0 \\ q_3 \end{pmatrix} = \begin{pmatrix} \frac{\sqrt{s}}{2} & \frac{\sqrt{s}}{2} \\ \frac{\sqrt{s}}{2} & -\frac{\sqrt{s}}{2} \end{pmatrix} \begin{pmatrix} \alpha \\ \beta \end{pmatrix}, \tag{2.32}$$

and q_\perp is a combination of transverse vectors. The jacobian is the absolute value of the determinant:

$$\left| \begin{array}{cc} \frac{\sqrt{s}}{2} & \frac{\sqrt{s}}{2} \\ \frac{\sqrt{s}}{2} & -\frac{\sqrt{s}}{2} \end{array} \right| = \left| -\frac{\sqrt{s}}{2} \frac{\sqrt{s}}{2} - \frac{\sqrt{s}}{2} \frac{\sqrt{s}}{2} \right| = \frac{s}{2}. \tag{2.33}$$

Then, all integrations over the four-momenta q can be written in terms of the Sudakov variables,

$$\int \frac{d^4 q}{(2\pi)^4} \rightarrow \frac{s}{2(2\pi)^2} \int \frac{d^2 q_\perp}{(2\pi)^2} d\alpha d\beta. \tag{2.34}$$

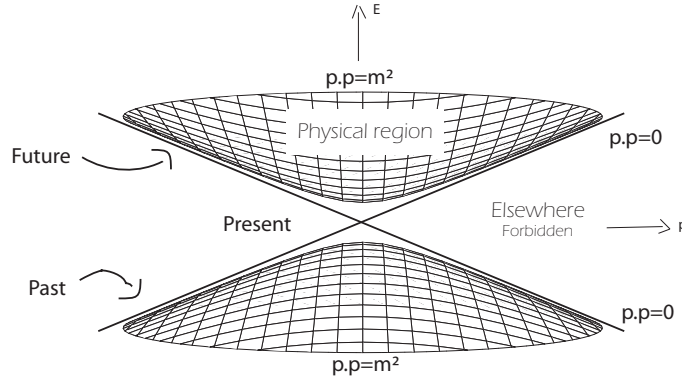


Figure 2.7: Light-cone in energy-momentum space.

Light-cone variables

Another property of Sudakov variables is that they are easily translated into variables on the light-cone for which there are some useful simplifications in calculations for high-energy scattering because of the presence of ultra-relativistic particles and of a preferred axis [33].

Firstly, let us remind the reader of the meaning of the light-cone. In the light-cone picture of Fig. 2.7, the envelope of the cone is the line $p.p = 0$, it is the trajectory of a massless particle in the energy-momentum diagram. Massive particles move on a hyperboloid inside the cone defined by $p.p = M^2$. In the high-energy limit i.e. for s large, the hyperboloid tends towards the light-cone. Usual light-cone coordinates are:

$$p_\mu = (p_+, p_-, p_\perp), \quad (2.35)$$

where⁶

$$p_+ = \frac{p_0 + p_3}{\sqrt{2}}, \quad p_- = \frac{p_0 - p_3}{\sqrt{2}}, \quad p_\perp = (p_1, p_2). \quad (2.36)$$

Note that these coordinates depend on the choice of the z -axis. The Lorentz invariant scalar product has the form

$$p.p = 2p_+p_- - \vec{p}_\perp^2 = M^2, \quad (2.37)$$

with the on-shell conditions, $p_+ > 0$ and $p_- > 0$. We loose the explicit dependence upon the square of the four-momentum, the only square quantity is \vec{p}_\perp^2 and we have a linear expression in p_+ or p_- in the denominators of the propagator.

Let us now take a look at the Sudakov variables. Because we want to use these variables in scattering processes, we define the z -axis as the natural direction of the collision as shown in Fig. 2.8. The four-momenta of the incoming particles are the same as in eq. (2.30) and eq. (2.31) and because of $q = \alpha p_1 + \beta p_2 + \vec{q}_\perp$ this means that

⁵See the next section for a more detailed study of this choice.

⁶Note that some authors omit the $\sqrt{2}$.

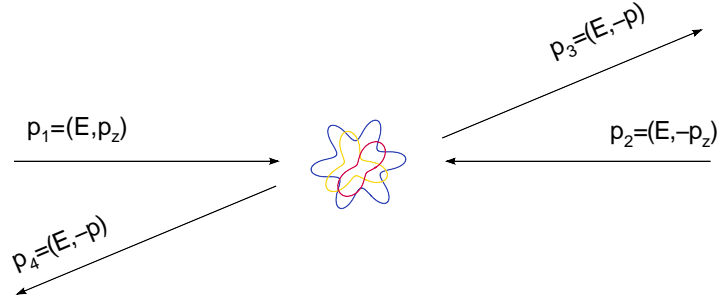


Figure 2.8: Usual kinematics in high-energy scattering processes.

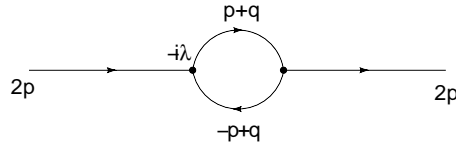
$$q_+ = q_0 + q_3 = \left(\alpha \frac{\sqrt{s}}{2} + \beta \frac{\sqrt{s}}{2}\right) + \left(\alpha \frac{\sqrt{s}}{2} + \beta \frac{-\sqrt{s}}{2}\right) = \alpha \sqrt{s}, \quad (2.38)$$

$$q_- = q_0 - q_3 = \left(\alpha \frac{\sqrt{s}}{2} + \beta \frac{\sqrt{s}}{2}\right) - \left(\alpha \frac{\sqrt{s}}{2} + \beta \frac{-\sqrt{s}}{2}\right) = \beta \sqrt{s}. \quad (2.39)$$

We immediately recognize the light-cone variables structure and their useful properties.

2.4 A complete calculation of a one-loop diagram

We will now perform a complete calculation of the diagram of Fig. 2.9 in order to illustrate the cutting rules. To make it easier, we begin in $\lambda\phi^3$ theory⁷ where all particles are scalar, the

Figure 2.9: A one loop diagram in $\lambda\phi^3$ theory.

coupling is λ and there is no trace in the numerator⁸. Firstly, we do the complete calculation with Sudakov variables. Secondly, we apply cutting rules to obtain the imaginary part of the diagram. We compare the results in the conclusion.

2.4.1 Complete calculation

We begin by computing the imaginary part of the diagram of Fig. 2.9 with no help from cutting rules.

The incoming and outgoing particles are massive and we suppose the quarks massless. We call $2p$ the four-momentum of the incoming particle, q the four-momentum in the loop, p_1 and p_2 are the light-cone vectors that we need for our Sudakov decomposition. The special Sudakov parametrization for q and p is,

⁷ $\lambda\phi^3$ theory is super-renormalizable in four dimensions then we do not have to worry about UV renormalization.

⁸We remind the reader of Feynman rules for $\lambda\phi^3$ and for other theories in Appendix B.

$$q = \alpha p_1 + \tilde{\beta} p_2 + q_\perp \quad (2.40)$$

$$p = p_1 + \frac{b}{s} p_2, \quad (2.41)$$

and we should not forget the jacobian at the end of the calculation⁹. The particular choice for the coefficient of p_2 in the p parametrization means that the incoming particle is essentially in the p_1 direction (on the light-cone) plus a small component in the p_2 direction. Mathematically and in a general way, if M is the mass of a particle,

$$\begin{aligned} p &= (E, \vec{0}, \sqrt{E^2 - M^2}) \sim (E, 0, E) + \mathcal{O}\left(\frac{1}{E}\right), \\ &\rightarrow p = p_1 + \frac{b}{s} p_2, \end{aligned} \quad (2.42)$$

in the high-energy limit. This allows us to write the four-momentum p equal to p_1 plus a small correction in order of $1/s$ because of the mass of the incoming particles. In this case and in the limit of high energy, we have the relations

$$p_1 \cdot p_1 = 0, \quad p_2 \cdot p_2 = 0, \quad p_1 \cdot p_2 = \frac{s}{2}. \quad (2.43)$$

as we explained in section 2.3. The momentum p is such as $4p^2 = M^2$, then

$$4p^2 = M^2 = b \quad \rightarrow \quad b = \frac{M^2}{4}. \quad (2.44)$$

In the rest of the calculation we will use

$$\frac{M^2}{4s} = \frac{\mu}{s} = \tilde{\mu}. \quad (2.45)$$

The diagram contains two four-momenta that can be written:

$$p + q = (\alpha + 1)p_1 + (\tilde{\beta} + \tilde{\mu})p_2 + q_\perp \quad (2.46)$$

$$-p + q = (\alpha - 1)p_1 + (\tilde{\beta} - \tilde{\mu})p_2 + q_\perp, \quad (2.47)$$

and the corresponding inverse propagators are

$$(p + q)^2 + i\epsilon = (\alpha + 1)(\tilde{\beta} + \tilde{\mu})s + q_\perp^2 + i\epsilon, \quad (2.48)$$

$$(-p + q)^2 + i\eta = (\alpha - 1)(\tilde{\beta} - \tilde{\mu})s + q_\perp^2 + i\eta. \quad (2.49)$$

The amplitude in Sudakov variables is:

$$\begin{aligned} i\mathcal{M} &= \int \frac{d^4 q}{(2\pi)^4} \frac{i^2(-i\lambda)^2}{[(p + q)^2 + i\epsilon][(-p + q)^2 + i\eta]} \\ &= \frac{\lambda^2}{8\pi^2} \int \frac{d^2 q_\perp}{(2\pi)^2} \int \frac{d\alpha d\tilde{\beta}}{[(\alpha + 1)(\tilde{\beta} + \tilde{\mu})s + q_\perp^2 + i\epsilon][(\alpha - 1)(\tilde{\beta} - \tilde{\mu})s + q_\perp^2 + i\eta]}. \end{aligned} \quad (2.50)$$

⁹The $\tilde{\beta}$ notation seems not useful but it will be justified by the following.

Poles in α

The first step is a study of the poles in the denominator. The quark propagators have poles at

$$\alpha_1 = \frac{-q_{\perp}^2 - i\epsilon}{s(\tilde{\beta} + \tilde{\mu})} - 1 \quad (2.51)$$

$$\alpha_2 = \frac{-q_{\perp}^2 - i\eta}{s(\tilde{\beta} - \tilde{\mu})} + 1. \quad (2.52)$$

The positions of the poles in function of the value of β in the α integral are shown in Fig. 2.10. We perform the integral by residue and constrain $\tilde{\beta}$ to lie between $-\tilde{\mu}$ and $\tilde{\mu}$: for

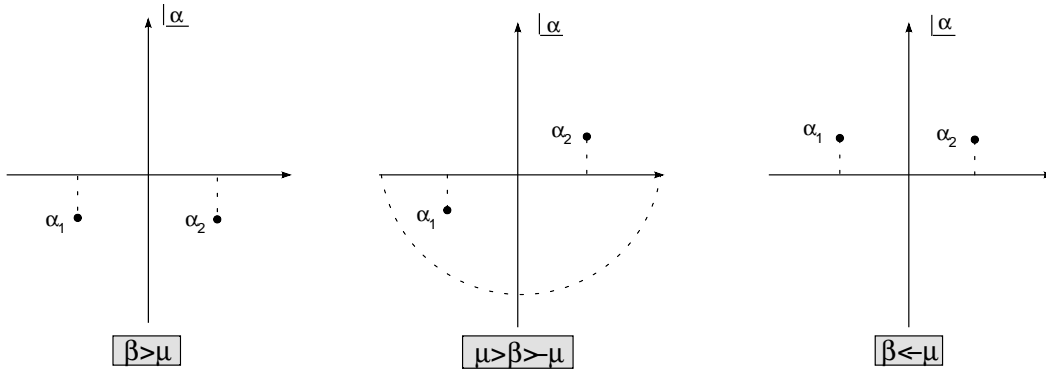


Figure 2.10: Position of the poles in the α integral in function of β .

other values of $\tilde{\beta}$, we can close the contour without enclosing any poles and the integral is zero. Consequently, we can consider $\tilde{\beta}$ small and of order $1/s$. We recall

$$\tilde{\beta} = \frac{\beta}{s}. \quad (2.53)$$

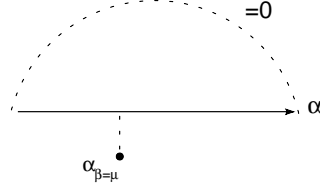
The new poles in α are

$$\alpha_1 = \frac{-q_{\perp}^2 - i\epsilon}{(\beta + \mu)} - 1, \quad (2.54)$$

$$\alpha_2 = \frac{-q_{\perp}^2 - i\eta}{(\beta - \mu)} + 1. \quad (2.55)$$

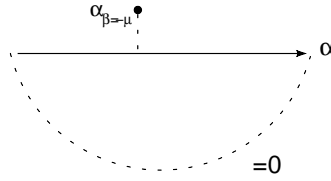
We have to be careful with these poles because we can have some problem if $\mu = 0$, $\beta = \mu$ and $\beta = -\mu$, the two last cases have poles at infinity. Then, we study the amplitude in these particular cases:

- $[\beta = \mu]$: the integrand in eq. (2.50) has one pole at $\alpha_{\beta=\mu} = \frac{-q_{\perp}^2 - 2\mu - i\epsilon}{\mu}$.
The amplitude is equal to zero because we can close the integration contour upward



and the pole will not contribute.

- $[\beta = -\mu]$: the integrand in eq. (2.50) has one pole at $\alpha_{\beta=-\mu} = \frac{q_{\perp}^2 + 2\mu + i\epsilon}{\mu}$.
We can close the integration contour downward, giving zero.



- $[\mu = 0]$: the interval $[-\mu, \mu]$ has zero measure and hence, at the threshold energy ($s = M/4=0$) there are no poles contributing to the amplitude.

We can conclude that the value $\beta = \mu$ and $\beta = -\mu$ don't contribute to the amplitude.

Let us now come back to the calculation, the amplitude (2.50) becomes

$$\mathcal{M} = -\frac{\lambda^2}{8\pi^2} \int \frac{d^2 q_{\perp}}{(2\pi)^2} \int_{-\mu}^{\mu} d\beta \oint_C f(\alpha) d\alpha, \quad (2.56)$$

with

$$f(\alpha) = \frac{1}{[(\alpha + 1)(\tilde{\beta} + \tilde{\mu}) + q_{\perp}^2 + i\epsilon][(\alpha - 1)(\tilde{\beta} - \tilde{\mu}) + q_{\perp}^2 + i\epsilon]}. \quad (2.57)$$

The integral over α is solved by Cauchy's theorem which we remind the reader of in Appendix A and we have

$$\oint_C f(\alpha) d\alpha = -2i\pi \text{Res}_{[\alpha=\alpha_1]} f(\alpha) + \int_{C_{\infty}} f(\alpha) d\alpha. \quad (2.58)$$

C_{∞} is the half semicircle drawn in the center of Fig. 2.10 but this integral vanishes¹⁰ because the integrand decreases faster than $1/\alpha$. By definition, the residue in α_1 is

$$\text{Res}_{[\alpha=\alpha_1]} = \lim_{\alpha \rightarrow \alpha_1} (\alpha - \alpha_1) f(\alpha) \quad (2.59)$$

Therefore, the contribution of the pole α_1 yields the integral,

$$\mathcal{M} = \frac{i\lambda^2}{4\pi} \int \frac{d^2 q_{\perp}}{(2\pi)^2} \int_{-\mu}^{\mu} d\beta \frac{1}{2[q_{\perp}^2 \mu - (\beta^2 - \mu^2 + i\epsilon)]}. \quad (2.60)$$

¹⁰In the intuitive way but we can easily prove it via the estimation lemma written in Appendix A.

Poles in β

Now, we have to study the new integrand

$$\mathcal{M} = \frac{i\lambda^2}{8\pi} \int \frac{d^2 q_{\perp}}{(2\pi)^2} \int_{-\mu}^{\mu} d\beta \frac{1}{[\beta^2 - \beta_0^2]}. \quad (2.61)$$

It has poles at

$$\begin{aligned} \beta_0 &= \pm \sqrt{\mu^2 + q_{\perp}^2 \mu}, \\ &= \pm \beta_0. \end{aligned} \quad (2.62)$$

We can associate each pole at each of the two pieces for the total amplitude drawn in Fig. 2.11. The parameters β is positive in $[0, \mu]$ for the first diagram and negative in $[-\mu, 0]$ for the second,

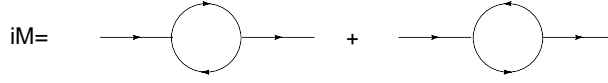


Figure 2.11: Total amplitude of the studied process.

the total amplitude is thus twice the amplitude of one of them. We now check the conditions for these poles to be in the domain of the β integration i.e. if $\mu^2 > \beta_0^2 > 0$.

$$\begin{aligned} 1. \quad & \mu^2 + q_{\perp}^2 \mu < \mu^2 \\ & q_{\perp}^2 < 0. \end{aligned} \quad (2.63)$$

$$\begin{aligned} 2. \quad & \mu^2 + q_{\perp}^2 \mu > 0 \\ & q_{\perp}^2 > -\mu. \end{aligned} \quad (2.64)$$

Hence, if $q_{\perp}^2 \in [-\mu, 0]$ there are poles in the domain of integration that contribute to the imaginary part of the amplitude.

First, we focus our attention on the imaginary part and because of the poles

$$\text{Im}(\mathcal{M}) = \frac{i\lambda^2}{8\pi} \int \frac{d^2 q_{\perp}}{(2\pi)^2} [(-i\pi)[\text{Res}_{[\beta=\beta_0]} - \text{Res}_{[\beta=-\beta_0]}]f(\beta)], \quad (2.65)$$

with

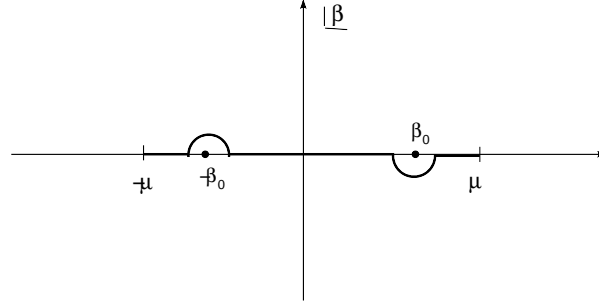
$$f(\beta) = \frac{1}{[\beta - \beta_0][\beta + \beta_0]} \quad (2.66)$$

along the integration contour shown in Fig. 2.12. We have

$$\text{Res}_{[\beta=\beta_0]} = \frac{1}{2\sqrt{\mu^2 + q_{\perp}^2 \mu}}, \quad (2.67)$$

$$\text{Res}_{[\beta=-\beta_0]} = \frac{-1}{2\sqrt{\mu^2 + q_{\perp}^2 \mu}}. \quad (2.68)$$

And then, the imaginary part of the amplitude is


 Figure 2.12: Positions of the pole in the β integral.

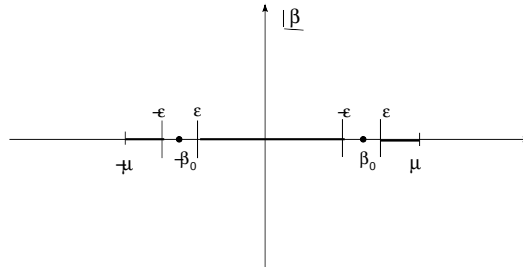
$$\text{Im}(\mathcal{M}) = \frac{\lambda^2}{4} \int \frac{d^2 q_{\perp}}{(2\pi)^2} \frac{1}{\sqrt{\mu^2 + q_{\perp}^2 \mu}}, \quad (2.69)$$

remember that q_{\perp}^2 is a negative quantity and the last integral over $d^2 q_{\perp}$ is not divergent.

$$\begin{aligned} \text{Im}(\mathcal{M}) &= \frac{\lambda^2}{4} \int \frac{dq_{\perp}^2 d\phi}{2(2\pi)^2} \frac{1}{\sqrt{\mu^2 - q_{\perp}^2 \mu}} \\ &= \frac{\lambda^2}{4} \pi \int_0^{\mu} \frac{dq_{\perp}^2}{(2\pi)^2} \frac{1}{\sqrt{\mu^2 - q_{\perp}^2 \mu}} \\ &= \frac{\lambda^2}{4} \pi \left. \frac{2\sqrt{\mu^2 - q_{\perp}^2 \mu}}{-\mu} \right|_0^{\mu} \\ &= \frac{\lambda^2}{8\pi}. \end{aligned} \quad (2.70)$$

Real part

The real part of the amplitude is calculated in two steps, the first is the principal part of eq. (2.60) corresponding to $q_{\perp}^2 \in [-\mu, 0]$, i.e. an integral along the real axis where we just remove the poles contribution calculated before. The second is an ordinary integral on β


 Figure 2.13: Principal part of the integral, we remove the pole contribution and take the limit $\epsilon \rightarrow 0$.

corresponding to $q_{\perp}^2 \in [-s, -\mu]$.

Let us begin with the principal part, by definition we have

$$\text{P} \int_{-\infty}^{\infty} \frac{f(x)}{x-x_0} dx = \lim_{\epsilon \rightarrow 0} \left[\int_{-\infty}^{x_0-\epsilon} + \int_{x_0+\epsilon}^{\infty} \right] \frac{f(x)}{x-x_0} dx, \quad (2.71)$$

where x_0 are the pole of the function $f(x)$. In our case, we have to compute

$$\text{P} \int_{-\mu}^{\mu} \frac{d\beta}{[\beta^2 - \beta_0^2]}, \quad (2.72)$$

with $\beta_0^2 = \mu^2 + q_{\perp}^2 \mu$ a positive quantity. After some transformations, we have to compute

$$\begin{aligned} \text{P} \int_{-\mu}^{\mu} \frac{d\beta}{[\beta^2 - \beta_0^2]} &= \text{P} \int_{-\mu}^{\mu} \frac{d\beta}{(\beta - \beta_0)(\beta + \beta_0)} \\ &= \text{P} \int_{-\mu}^{\mu} \frac{d\beta}{2\beta_0} \left[\frac{1}{(\beta - \beta_0)} - \frac{1}{(\beta + \beta_0)} \right] \\ &= \text{P} \int_{-\mu}^{\mu} \frac{d\beta}{2\beta_0} \left[\frac{1}{(\beta - \beta_0)} - \frac{-1}{(\beta - \beta_0)} \right] \\ &= \frac{1}{\beta_0} \text{P} \int_{-\mu}^{\mu} \frac{d\beta}{(\beta - \beta_0)}. \end{aligned} \quad (2.73)$$

The principal part is

$$\text{P} \int_{-\mu}^{\mu} \frac{d\beta}{(\beta - \beta_0)} = \lim_{\epsilon \rightarrow 0} \left[\int_{-\mu}^{-\beta_0-\epsilon} + \int_{\beta_0+\epsilon}^{\mu} \right] \frac{d\beta}{\beta - \beta_0} = \ln \left(\frac{\mu - \beta_0}{\mu + \beta_0} \right). \quad (2.74)$$

The first branch of the real part is thus

$$\frac{2\pi}{\sqrt{\mu^2 + q_{\perp}^2 \mu}} \int_{-\mu}^0 \frac{d^2 q_{\perp}}{(2\pi)^2} \ln \left(\frac{\mu - \sqrt{\mu^2 + q_{\perp}^2 \mu}}{\mu + \sqrt{\mu^2 + q_{\perp}^2 \mu}} \right). \quad (2.75)$$

The second branch with $q_{\perp}^2 \in [-\infty, -\mu]$ can be integrated directly because there is no pole in the denominator,

$$\int_{-\mu}^{\mu} \frac{d\beta}{\beta^2 + |\beta_0^2|} = \int_{-\mu}^{\mu} \frac{1}{|\beta_0^2|} \frac{d\beta}{\frac{\beta^2}{|\beta_0^2|} + 1}, \quad (2.76)$$

with $|\beta_0^2| = -\mu^2 - q_{\perp}^2 \mu$ then we have

$$\begin{aligned} \int_{-\mu}^{\mu} \frac{d\beta}{\beta^2 + |\beta_0^2|} &= \frac{1}{|\beta_0|} \tan^{-1} \left(\frac{\beta}{\beta_0} \right) \Big|_{-\mu}^{\mu} \\ &= \frac{1}{|\beta_0|} \tan^{-1} \left(\frac{\mu}{\beta_0} \right) - \tan^{-1} \left(\frac{-\mu}{\beta_0} \right) \\ &= \frac{2}{\sqrt{\mu^2 + q_{\perp}^2 \mu}} \tan^{-1} \left(\frac{\mu}{\sqrt{\mu^2 + q_{\perp}^2 \mu}} \right). \end{aligned} \quad (2.77)$$

and the second branch is

$$\frac{4\pi}{\sqrt{\mu^2 + q_\perp^2} \mu} \int_{-\infty}^{-\mu} \frac{d^2 q_\perp}{(2\pi)^2} \tan^{-1} \left(\frac{\mu}{\sqrt{\mu^2 + q_\perp^2} \mu} \right). \quad (2.78)$$

We now have the real part of the amplitude,

$$\begin{aligned} \text{Re}(\mathcal{M}) = & \frac{2\pi}{\sqrt{\mu^2 + q_\perp^2} \mu} \left[\int_{-\mu}^0 \frac{d^2 q_\perp}{(2\pi)^2} \ln \left(\frac{\mu - \sqrt{\mu^2 + q_\perp^2} \mu}{\mu + \sqrt{\mu^2 + q_\perp^2} \mu} \right) \right. \\ & \left. + 2 \int_{-s}^{-\mu} \frac{d^2 q_\perp}{(2\pi)^2} \tan^{-1} \left(\frac{\mu}{\sqrt{\mu^2 + q_\perp^2} \mu} \right) \right]. \end{aligned} \quad (2.79)$$

2.4.2 Cutting rules calculation

We now apply cutting rules and compute directly the imaginary part of the amplitude via the discontinuity of the diagram 2.9. We use the Sudakov parametrization and because of our previous study, we know that β is of order $1/s$ and we directly use it in

$$q = \alpha p_1 + \frac{\beta}{s} p_2 + q_\perp. \quad (2.80)$$

We cut through the diagram in all possible ways, in this case there is only one possible cut as we show in Fig. 2.14, and put on-shell the cut propagators,

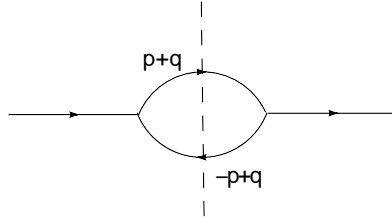


Figure 2.14: Cut in the studying diagram.

$$(\alpha + 1)(\beta + \mu) + q_\perp^2 = 0, \quad (2.81)$$

$$(\alpha - 1)(\beta - \mu) + q_\perp^2 = 0. \quad (2.82)$$

For each cut, we replace the propagator by a δ -function and perform the loop integral. In practice, this means to solve this system of equation for α and β and to replace them in the expression of the amplitude,

$$i\mathcal{M} = \frac{\lambda^2}{8\pi^2} \int \frac{d^2 q_\perp}{(2\pi)^2} \int \frac{d\beta d\alpha}{[(\alpha + 1)(\tilde{\beta} + \tilde{\mu}) + q_\perp^2 + i\epsilon][(\alpha - 1)(\tilde{\beta} - \tilde{\mu}) + q_\perp^2 + i\eta]}. \quad (2.83)$$

Before applying the cutting rules, we check the condition of application: energy in the loop must be positive. We use two methods, the first is to argue that if energy is positive, the components of the corresponding four-momenta are positive and thus

$$\begin{aligned}\alpha + 1 &> 0, \\ \beta + \mu &> 0,\end{aligned}\tag{2.84}$$

for the $(p + q)$ four-momentum. The $(-p + q)$ four-momentum corresponds to an antiquark hence the conditions become

$$\begin{aligned}\alpha - 1 &< 0, \\ \beta - \mu &< 0.\end{aligned}\tag{2.85}$$

This constrains α and β to lie between

$$-1 < \alpha < 1,\tag{2.86}$$

$$-\mu < \beta < \mu.\tag{2.87}$$

We can also calculate a quantity proportional to the energy,

$$(p + q) \cdot p = (\alpha + 1)\mu \frac{s}{2} + \left(\frac{\beta + \mu}{s}\right) \frac{s}{2},\tag{2.88}$$

$$(-p + q) \cdot p = (\alpha - 1)\mu \frac{s}{2} + \left(\frac{\beta - \mu}{s}\right) \frac{s}{2},\tag{2.89}$$

and impose it to be positive (negative for the antiquark) in the large s limit. The conditions are identical and we draw the physical region for the parameters in Fig. 2.15. As for q_{\perp}^2 ,

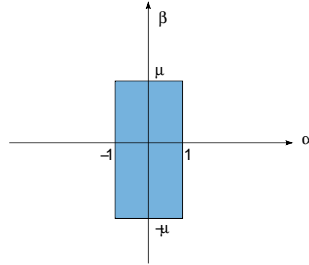


Figure 2.15: Physical region for the α and β parameters.

the kinematics constrains it to be smaller than something of order s because we cannot have more energy in the loop than in the incoming particles.

We now calculate the α integral via the first cut,

$$\text{Disc}\mathcal{M} = \frac{\lambda^2}{8\pi^2} \int \frac{d^2q_{\perp}}{(2\pi)^2} \int d\beta \int \frac{d\alpha}{[(\alpha - 1)(\beta - \mu) + q_{\perp}^2]} \times (-2\pi)\delta(\alpha - \alpha_0),\tag{2.90}$$

with α_0 the solution of eq. (2.81):

$$\alpha_0 = \frac{-q_{\perp}^2}{(\beta + \mu)} - 1.\tag{2.91}$$

We put $\alpha = \alpha_0$ in the second equation (2.82) and solve it,

$$\begin{aligned} \left[\frac{-q_{\perp}^2}{\beta + \mu} - 2 \right] (\beta - \mu) + q_{\perp}^2 &= 0, \\ -q_{\perp}^2 (\beta - \mu) - 2(\beta^2 - \mu^2) + -q_{\perp}^2 (\beta + \mu) &= 0, \\ q_{\perp}^2 \mu - (\beta^2 - \mu^2) &= 0, \end{aligned} \tag{2.92}$$

that leads to

$$\beta = \pm \sqrt{\mu^2 + q_{\perp}^2 \mu}. \tag{2.93}$$

The pole β must be real and this constrains q_{\perp}^2 to lie between $-\mu$ and 0. One of the poles corresponds to the diagram that we study and the other one is the second cut of the diagram with arrows in the opposite direction as we explained in Section 2.4.1. The total amplitude is obviously the sum of both terms. Noting $\beta_0 = \sqrt{\mu^2 + q_{\perp}^2 \mu}$,

$$\begin{aligned} \text{Disc}\mathcal{M} &= \frac{\lambda^2}{8\pi} \int \frac{d^2 q_{\perp}}{(2\pi)^2} \int d\beta \left[\frac{-2\pi\delta(\beta - \beta_0)}{[\beta - \beta_0]} + \frac{2\pi\delta(\beta + \beta_0)}{[\beta + \beta_0]} \right], \\ &= \frac{\lambda^2}{2} \int \frac{d^2 q_{\perp}}{(2\pi)^2} \left[\frac{1}{2\sqrt{\mu^2 + q_{\perp}^2 \mu}} + \frac{1}{2\sqrt{\mu^2 + q_{\perp}^2 \mu}} \right] \\ &= \frac{\lambda^2}{2} \int \frac{d^2 q_{\perp}}{(2\pi)^2} \frac{1}{\sqrt{\mu^2 + q_{\perp}^2 \mu}}. \end{aligned} \tag{2.94}$$

for $\beta > 0$. The imaginary part of the amplitude is half the discontinuity of the diagram then

$$\text{Im}\mathcal{M} = \frac{\lambda^2}{4} \int \frac{d^2 q_{\perp}}{(2\pi)^2} \frac{1}{\sqrt{\mu^2 + q_{\perp}^2 \mu}}, \tag{2.95}$$

with q_{\perp}^2 a negative quantity.

We immediately see that the imaginary part computed by cutting rules in eq. (2.95) is exactly the same as the one computed completely in eq. (2.69).

2.4.3 The REDUCE version

This kind of calculation is easy to perform on the back of an envelope, this is a one-loop diagram. We want to use it as a foundation to more complicated diagrams with additional loops, intermediate states and other subtleties so that we write a small REDUCE program in order to help us in the calculation.

This program is very simple but can be used for more complex case that maybe need more than an envelope. The structure is always the same:

1. A common part with the definition of variables, vectors and the trace in the numerator.
2. The complete calculation of the amplitude with poles, residues and integration.
3. The amplitude calculation by cutting rules.

We write the program corresponding to the previous calculation with some comments in Appendix C.1. Others programs used in this work can be found in the appendix too.

2.5 Conclusion

Now, we have a better understanding of why the imaginary part is the basis of the problem in amplitude calculation, this part leads to the total amplitude and measurable quantities such as the total cross section through known relations. We have seen that cutting rules are a powerful tool in the calculation of the imaginary part of Feynman diagrams. Using them allows us to simplify calculations. In the following, we sometimes check results obtained by cutting rules by performing the complete calculation as a good exercise to understand the *inside* well of the calculus.

Chapter 3

Diffractive pomeron physics

This work introduces the basic tools for the calculation of the diffractive cross section for the production of a Higgs boson or another exotic particles. An example of a possible diagram is the one shown in Fig. 3.1. This diagram contains at least three loops and the two quark-loops

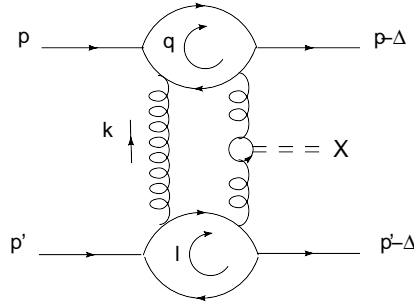


Figure 3.1: An example of diagram related to the diffractive cross section for the production of a Higgs boson in the high-energy limit.

are interpreted as the impact factor of the colliding proton or of other incoming hadrons. This is a complex problem so that we begin by a simpler case in order to understand the logics of this kind of calculation.

In this chapter, we start with a brief introduction of pomeron physics, the main ingredient in our calculation. We define the pomeron and explain where it dominates the amplitude. We then develop a method of calculation, introduce some simplification as k_{\perp} factorization and we interpret the pieces of the answer as physical objects. The last section is devoted to a simple diffractive calculation. We conclude by the outlook and the possible improvements.

3.1 An introduction to the pomeron

It was observed experimentally that the total cross section rises slowly as s increases. This rise can be explained by the exchange of a single Regge pole from a new trajectory called the Pomeron from its inventor Pomeranchuk [34]. In order to study scattering processes at the LHC, we have to know more about gluon exchanges which produce this pomeron.

The pomeron is whatever is exchanged between hadrons to make the approximately constant

total cross section that is observed at high energy [35]. It is an exchange of a color singlet¹ with vacuum quantum numbers that can be modeled most simply by the exchange of two (non)perturbative gluons² between a pair of quark and we show the simplest contribution in Fig. 3.2. The pomeron constitutes an excellent phenomenological description of hadronic



Figure 3.2: Simplest contribution to a pomeron exchange between quarks.

total cross sections, especially at high energy because at 1800 GeV more than 99% of the total cross section is due to pomeron exchange [8]. Another advantage is that high-energy hadronic diffractive processes that include pomeron exchanges usually lead to large rapidity gaps which is a beautiful tool of detection as we explain in the first chapter. Then, the pomeron seems to be an essential element in high-energy diffraction processes but there is still a need for a more fundamental understanding of its exact nature.

The pomeron is needed because we work at high energy where its trajectory dominates but also because it can lead to Higgs production. Actually, most of the models for Higgs, or exotic particles production in a rapidity gap are extension of the original paper by Bialas and Landshoff [20] where the Higgs is produced via a top quark loop and a minimum of two-gluon exchange, as in Fig 3.1. Hence, this lowest-order diagram is a good beginning in our understanding of diffractive Higgs production.

3.2 Calculation organization

In order to develop and test a method for loop calculations, we first define variables, tools and prepare a REDUCE program capable of doing the calculation. We start with a simplified case where the incoming particles are scalar mesons and two essentially transverse gluons, allowed by k_{\perp} factorization. In this section, we will justify this factorization and develop the method of calculation. We finish by explaining what will be the steps needed in order to change this calculation into an amplitude for Higgs-boson diffractive production.

3.2.1 k_{\perp} factorization

k_{\perp} factorization can be illustrated by the calculation of a simple two-gluon exchange. We will perform the beginning of the calculation and show that gluons are basically transverse in the large- s limit with their other components α and β being of order $1/s$.

The leading order of two-gluon singlet exchange contains the two simple diagrams drawn in Fig. 3.3, the first is called the direct diagram and the second the crossed diagram. We suppose the intermediate quarks and the incoming particles massless with $p_1^2 = p_2^2 = 0$ and the momentum transfer Δ null, i.e. the four-momenta of the incoming and outgoing quarks are the same³. In terms of Sudakov variables,

¹There is no color transferred between the incoming and outgoing quarks.

²A detailed approach has to make the difference between soft and hard pomerons. The reader can find a discussion about this topic in most of the references and especially in [36].

³This cannot be the case in Higgs diffractive production but we just want to have an idea of the parameters in the calculation.

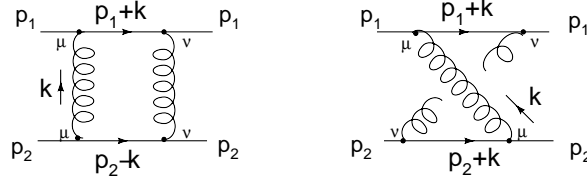


Figure 3.3: Lowest-order Feynman diagrams of a two-gluon exchange.

$$k = \alpha_k p_1 + \beta_k p_2 + k_\perp, \quad (3.1)$$

with the jacobian of this change of variable equal to $s/2$. We have the relations

$$p_1 \cdot k_\perp = 0, \quad (3.2)$$

$$p_2 \cdot k_\perp = 0, \quad (3.3)$$

$$p_1 \cdot p_2 = s/2, \quad (3.4)$$

in the large- s limit. We write the amplitudes where g_s is the coupling constant for the quark/gluon vertices,

$$i\mathcal{M} = (-ig_s)^4 C \int \frac{dk_\perp^2}{(2\pi)^4} \frac{\text{Tr}[\not{p}_1 \gamma^\nu (\not{p}_1 + \not{k}) \gamma^\mu] \text{Tr}[\not{p}_2 \gamma^\mu (\not{p}_2 - \not{k}) \gamma^\nu]}{[(p_1 + k)^2 - m_q^2 + i\epsilon][p_2 - k)^2 - m_q^2 + i\eta][k^2 + i\sigma]^2}, \quad (3.5)$$

$$i\mathcal{M}_c = (-ig_s)^4 C \int \frac{dk_\perp^2}{(2\pi)^4} \frac{\text{Tr}[\not{p}_1 \gamma^\nu (\not{p}_1 + \not{k}) \gamma^\mu] \text{Tr}[\not{p}_2 \gamma^\mu (\not{p}_2 + \not{k}) \gamma^\nu]}{[(p_1 + k)^2 - m_q^2 + i\epsilon][(p_2 + k)^2 - m_q^2 + i\eta_c][k^2 + i\sigma]^2}, \quad (3.6)$$

where we denote with a c index the element related to the crossed diagram, $C=2/9$ is the color factor where the 9 comes from the average over the color. We integrate eq. (3.5) by residue⁴ and then we study the denominator. It has poles in β at

$$\begin{aligned} (p_1 + k)^2 + i\epsilon &= (\alpha + 1)\beta s + k_\perp^2 + i\epsilon = 0 \\ &\rightarrow \beta_1 = \frac{-k_\perp^2 - i\epsilon}{(\alpha + 1)s}, \end{aligned} \quad (3.7)$$

$$\begin{aligned} (p_2 - k)^2 + i\eta &= (1 - \beta)\alpha s - k_\perp^2 + i\eta = 0 \\ &\rightarrow \beta_2 = \frac{k_\perp^2 - i\eta}{\alpha s} - 1, \end{aligned} \quad (3.8)$$

$$\begin{aligned} (p_2 + k)^2 - m^2 + i\eta_c &= (1 + \beta)\alpha s + k_\perp^2 + i\eta_c = 0 \\ &\rightarrow \beta_{2c} = \frac{-k_\perp^2 - i\eta_c}{\alpha s} - 1, \end{aligned} \quad (3.9)$$

$$\begin{aligned} k^2 + i\sigma &= \alpha\beta s + k_\perp^2 + i\sigma = 0 \\ &\rightarrow \beta_3 = \frac{-k_\perp^2 - i\sigma}{\alpha s}. \end{aligned} \quad (3.10)$$

Now, we study the position of the poles in function of the value of α in Fig 3.4. We can see

⁴We can solve the integral by cutting rules because the two intermediate quarks can simultaneously go on-shell. In this case, because the poles are simple and in order to understand well the parameters, we will perform the complete calculation.

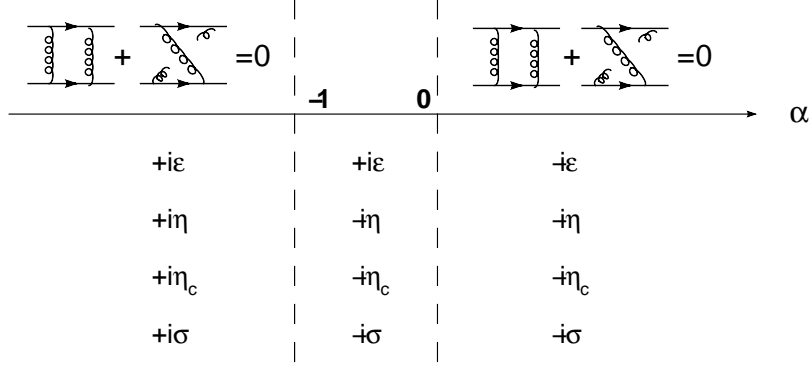


Figure 3.4: Position of the poles in the complex α plane in the function of the value of α .

that the physical region for α is between -1 and 0 where only the pole β_1 contributes and we can conclude that because of these only possible values for α , eq. (3.7) gives us a pole of order $1/s$. For other values of α , all the poles are on the same side of the real axis and we can closed the integration contour without including any pole so that the contribution to the amplitude is equal to zero. The change of variable gives us

$$\int \frac{d^4 k_\perp}{(2\pi)^4} \rightarrow \frac{s}{2(2\pi)^2} \int \frac{d\alpha d\beta dk_\perp^2}{(2\pi)^2}, \quad (3.11)$$

and the α -integral I_α becomes

$$I_\alpha = \int_{-1}^0 \text{Res}_{\beta_1}[f(\alpha, \beta, k_\perp^2)] d\alpha, \quad (3.12)$$

where Res_{β_1} is the residue in β_1 of the function $f(\alpha, \beta, k_\perp^2)$. We consider that α is small and remove the terms that contains α^2 then the new integrand has one pole at

$$\alpha = \frac{k_\perp^2}{s}. \quad (3.13)$$

This pole is of order $1/s$ and lies in the domain of integration if

$$-s < k_\perp^2 < 0. \quad (3.14)$$

This constrains $|k_\perp^2|$ below s with $k_\perp^2 < 0$. We can integrate directly over α by residue in order to obtain the contribution of the pole to the imaginary part of the amplitude. The cross diagram is calculated in the same way and the complete result in the large- s limit is

$$\mathcal{M} = ig_s^4 s C \int \frac{d^2 k_\perp}{(2\pi)^2} \frac{1}{k_\perp^4}. \quad (3.15)$$

This answer is in agreement with the Cheng and Wu result [37] and reference [3]. It is a purely imaginary contribution coming from the exact cancelation of the real part of the two lowest-order leading diagrams. We can directly impose the order $1/s$ of the pole on α and β parameters in our parametrization of k ,

$$k = \frac{\alpha_k}{s} p_1 + \frac{\beta_k}{s} p_2 + k_\perp \approx k_\perp. \quad (3.16)$$

This is the basis of k_\perp factorization and this physically means that the two gluons exchanged are principally transverse with only a small component in the p_1 and p_2 directions. It is

a useful property because it really simplifies the calculation in high-energy limit where $1/s$ terms can be ignored.

3.2.2 Intermediate quarks

The decomposition of the intermediate quark four-momentum in its Sudakov variables is motivated by the following physical argument.

We consider a collision where two scalar mesons come from opposite directions p_1 and p_2 . The mesons contain two quarks and we suppose that these quarks remain more or less in the same direction as the initial particles. Actually this is justified by the fact that the meson moves faster in the z direction taking with it the quarks so that the dominant quark velocity direction is the direction of the meson [2]. This can be seen in Fig. 3.5. Hence, we can write

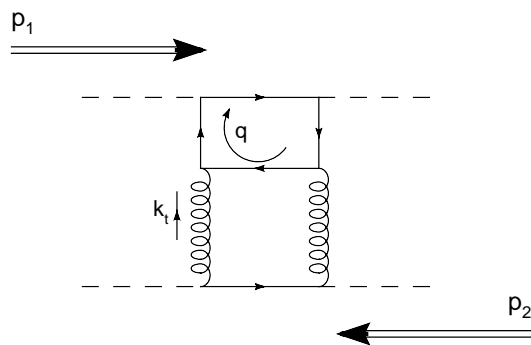


Figure 3.5: p_1 and p_2 direction and the q four-momentum parametrization interpretation.

the four-momentum q as

$$q = \alpha_q p_1 + \frac{\beta_q}{s} p_2 + q_\perp, \quad (3.17)$$

in the upper-quark loop of the diagram and

$$l = \frac{\alpha_l}{s} p_1 + \beta_l p_2 + l_\perp, \quad (3.18)$$

in the lower loop. This is the parametrization that we shall use in the rest of this work.

3.2.3 Method and physical interpretation

Now, we define the structure of the next calculation and the way we want to organize the answer in order to have a physical interpretation of the process.

We first consider a very simple case where we replace the proton by a scalar with no structure i.e. the transition vertex scalar/quark is simply a constant. In order to compute a physical amplitude and respect the gauge invariance of QCD, we have to consider all possible diagrams: this means compute the six diagram in Fig. 3.6. These are two-loop diagrams and we use k_\perp factorization and the parameterizations explained previously. We shall write the amplitude in a factorized form:

$$\int d^2 k_\perp f(k_\perp) \times \mathcal{F}(k_\perp). \quad (3.19)$$

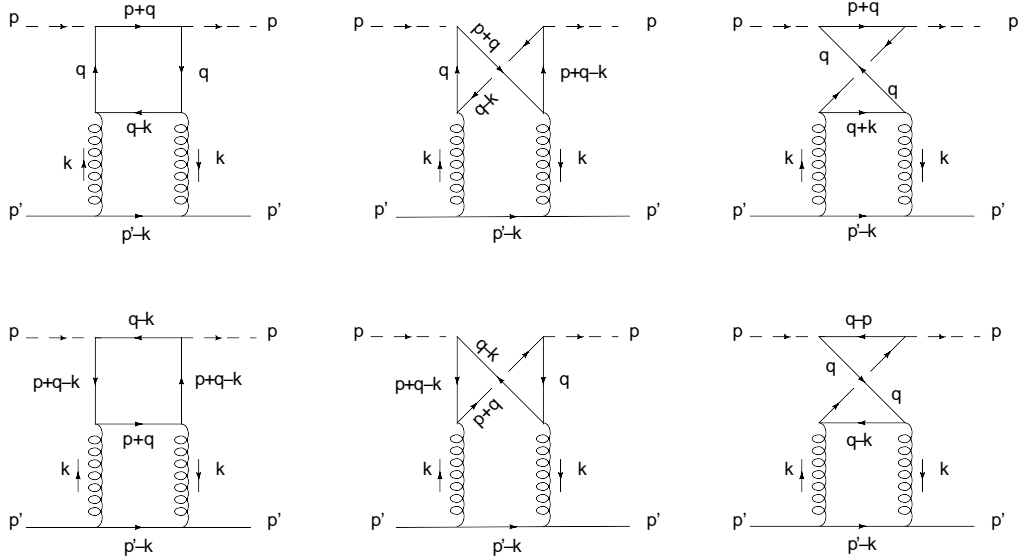


Figure 3.6: The six diagrams that contribute to the amplitude.

The \mathcal{F} function is the impact factor of the incoming particle and f is the usual amplitude of two-gluon exchange. This is what we expect from factorization, a separation between

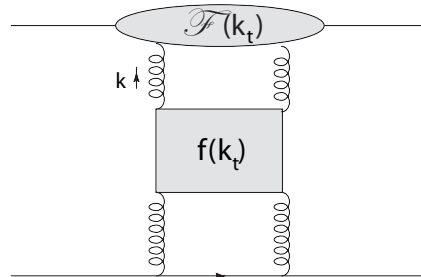


Figure 3.7: Physical interpretation of the factorization of eq. (3.19).

different parts of the dynamics of the scattering process. This interpretation is shown in Fig. 3.7. It is useful because it can be extended to more complicated cases by a modification of the impact factors alone. Each piece can be complicated without modifying the others.

Now, we have our tools and the expected form of the answer, with their help we can calculate the first step towards Higgs boson diffractive production.

3.3 A simple impact factor

The first step of the calculation is to introduce a quark loop in the upper part of the pomeron diagram of Fig. 3.3 and to compute the corresponding amplitude. According to Feynman rules, the amplitude is the sum of all possible ways to draw the same process with Feynman diagrams. Remember that we work in the high-energy limit so that we can neglect terms

of order $1/s$. We begin by computing the imaginary part of the amplitude via cutting rules on the two first diagrams (a) and (b) shown in Fig. 3.8 with obviously the same diagrams

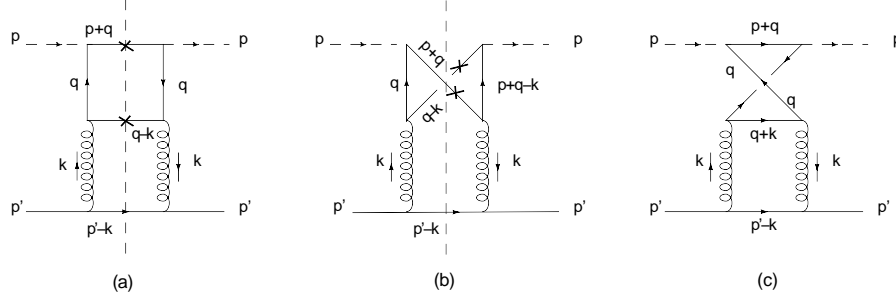


Figure 3.8: The three diagrams that contribute to the amplitude. Diagram (c) cannot be cut and lead to a totally real contribution. We shall add later the three same diagrams with arrows in the opposite direction.

with arrows in the opposite direction. The kinematics is arranged so they have the same intermediate states. The last possible diagram (c) cannot be cut and leads to a totally real contribution which does not contribute to the imaginary part. We further simplify the calculation by considering only the contribution at $t=0$.

We use the Sudakov parametrization so that the intermediate quarks and exchanged gluons four-momenta are

$$q = \alpha_q p_1 + \frac{\beta_q}{s} + q_\perp, \quad (3.20)$$

$$k = \frac{\alpha_k}{s} p_1 + \frac{\beta_k}{s} + k_\perp, \quad (3.21)$$

with k_\perp and q_\perp in (3.2). The incoming particles are denoted by p and p' and supposed to move very close to the p_1 and p_2 direction respectively, then

$$p = p_1 + b p_2, \quad (3.22)$$

$$p' = a p_1 + p_2. \quad (3.23)$$

Here we consider the incoming particles massive with a mass M . On the light-cone, we have $p^2 = p'^2 = M^2$ and this can be used to determine the parameters a and b .

$$p^2 = 2b p_1 \cdot p_2 = 2b \frac{s}{2} = b s = M^2, \quad (3.24)$$

$$\rightarrow p = p_1 + \frac{M^2}{s} p_2.$$

$$p'^2 = 2a p_1 \cdot p_2 = 2a \frac{s}{2} = a s = M^2, \quad (3.25)$$

$$\rightarrow p' = \frac{M^2}{s} p_1 + p_2.$$

We rename $M^2 = \mu$ and express the quark four-momenta in terms of the new variables,

$$p + q = (\alpha_q + 1)p_1 + \frac{(\beta_q + \mu)}{s}p_2 + q_\perp, \quad (3.26)$$

$$q - k = (\alpha_q - \frac{\alpha_k}{s})p_1 + \frac{(\beta_q - \beta_k)}{s}p_2 + (q_\perp - k_\perp), \quad (3.27)$$

$$p' - k = \frac{(\mu - \alpha_k)}{s}p_1 + (1 - \frac{\beta_k}{s})p_2 - k_\perp, \quad (3.28)$$

$$q - k + p = (\alpha_q - \frac{\alpha_k}{s} + 1)p_1 + \frac{(\beta_q - \beta_k + \mu)}{s}p_2 + (q_\perp - k_\perp). \quad (3.29)$$

The corresponding denominators of the six propagators in the large- s limit are

$$(p + q)^2 = (\alpha_q + 1)(\beta_q + \mu) + q_\perp^2, \quad (3.30)$$

$$(q - k)^2 \simeq \alpha_q(\beta_q - \beta_k) + (q_\perp - k_\perp)^2, \quad (3.31)$$

$$(p' - k)^2 \simeq (\mu - \alpha_k) + k_\perp^2, \quad (3.32)$$

$$(q - k + p)^2 = (\alpha_q + 1)(\beta_q - \beta_k + \mu) + (q_\perp - k_\perp)^2, \quad (3.33)$$

and

$$q^2 = \alpha_q\beta_q + q_\perp^2, \quad (3.34)$$

$$k^2 \simeq k_\perp^2. \quad (3.35)$$

The imaginary part of the amplitude is obtained by cutting rule under the condition of positive energy in the loop:

$$\begin{aligned} (p + q) \cdot (k - q) &> 0 & (p + q) \cdot p &> 0 \\ (p + q) \cdot (p' - k) &> 0 & (p' - k) \cdot p &> 0 \\ (q - k) \cdot (p' - k) &> 0 & (q - k) \cdot p &> 0 \end{aligned} \quad (3.36)$$

Hence, the upper limit on q_\perp^2 and k_\perp^2 is of order s and we will use s as the limit in the rest of the calculation. We can also evaluate the domain of the variable α_q by the physical interpretation of the Sudakov parametrization since the coefficients of p_1 and p_2 have to be positive for quarks and negative for antiquarks. For example, in

$$p + q = (\alpha_q + 1)p_1 + \frac{(\beta_q + \mu)}{s}p_2 + q_\perp, \quad (3.37)$$

we need

$$\alpha_q + 1 > 0, \quad (3.38)$$

$$\beta_q + \mu > 0. \quad (3.39)$$

By applying this to the three cut propagators, we find

$$\begin{aligned} -1 &< \alpha_q < 0 \\ \mu &< \beta_q < \beta_k \\ 0 &< \alpha_k < \mu \\ \beta_q &< \beta_k < s \end{aligned} \quad (3.40)$$

We will use these conditions in the last integration on α_q .

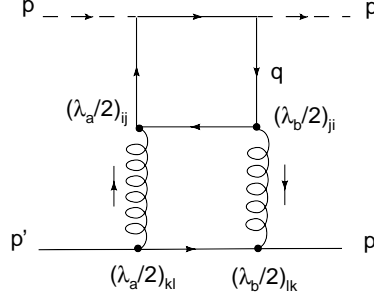


Figure 3.9: Notation in order to compute the color factor.

Color factor

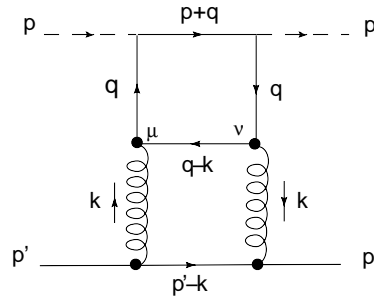
The color factor of the diagram C is (see Fig. 3.9)

$$\begin{aligned}
 C &= \sum_{abc} \left(\frac{\lambda_a}{2}\right)_{ji} \left(\frac{\lambda_b}{2}\right)_{ij} \left(\frac{\lambda_a}{2}\right)_{kl} \left(\frac{\lambda_b}{2}\right)_{lk} \\
 &= Tr\left(\frac{\lambda_a}{2} \frac{\lambda_b}{2}\right) Tr\left(\frac{\lambda_a}{2} \frac{\lambda_b}{2}\right) \\
 &= \frac{1}{4} \delta_{aa} \\
 &= 2.
 \end{aligned} \tag{3.41}$$

Let us now compute the six diagrams that contribute to the impact factor.

Diagram a

First we study the diagram (a) drawn in Fig. 3.10. The intermediate quarks are massless,

Figure 3.10: First piece of the amplitude: M_{a1} .

$m_q = 0$, the coupling constant is g at the scalar vertices and g_s at the quark/gluon vertices. According to Feynman rules the amplitude is

$$M_{a1} = (-ig_s)^2 C \int \frac{d^4 k}{(2\pi)^4} \frac{Tr[\not{p}' \gamma^\nu (\not{p}' - \not{k}) \gamma^\mu]}{[(p' - k)^2 + i\eta][k^2 + i\sigma]^2} \times Q_{a1}(q). \tag{3.42}$$

with $Q_{a1}(q)$ comes from the quark loop,

$$Q_{a1}(q) = (-1)(-ig)^2 (-ig_s)^2 \int \frac{d^4 q}{(2\pi)^4} \frac{Tr[(\not{p} + \not{q}) \not{q} \gamma^\mu (\not{q} - \not{k}) \gamma^\nu \not{q}]}{[(p + q)^2 + i\epsilon][q^2 + i\rho]^2 [(q - k)^2 + i\delta]}. \tag{3.43}$$

We express the amplitude in terms of the Sudakov variables and replace the three cut propagators by a δ -function to obtain the discontinuity of the diagram,

$$\text{Disc}(M_{a1}) = g_s^2 \frac{C}{2s(2\pi)^2} \int \frac{d\alpha_k d\beta_k d^2 k_\perp}{(2\pi)^2} \frac{N_2}{[k_\perp^2]^2} 2\pi\delta[(p' - k)^2] \times Q(\alpha_q, \beta_q, q_\perp^2), \quad (3.44)$$

$$Q_{a1}(\alpha_q, \beta_q, q_\perp^2) = g_s^2 g^2 \frac{1}{2(2\pi)^2} \int \frac{d\alpha_q d\beta_q d^2 q_\perp}{(2\pi)^2} \frac{N_1}{[\alpha_q \beta_q + q_\perp^2]^2} \times 2\pi\delta[(p+q)^2] 2\pi\delta[(q-k)^2]. \quad (3.45)$$

The numerators N_1 and N_2 are the traces on the fermion lines that we compute with the help of REDUCE. We first perform the loop integral and give the details for one of the δ -functions because the method is the same for the others. We have

$$\begin{aligned} \delta[(p+q)^2] &= \delta[(\alpha_q + 1)(\beta_q + \mu) + q_\perp^2] \\ &= \delta[\beta_q - (\frac{-q_\perp^2}{\alpha_q + 1} - \mu)] \frac{1}{\alpha_q + 1}, \end{aligned} \quad (3.46)$$

where the last fraction is the jacobian of the δ -function coming from the property

$$\delta(ax) = \frac{1}{|a|} \delta(x). \quad (3.47)$$

Performing the integral over β_q is equivalent to replacing β_q by $(\frac{-q_\perp^2}{\alpha_q + 1} - \mu)$ in the expression of the amplitude. Hence we obtain

$$\begin{aligned} \text{Disc} M_{a1} &= -g_s^2 \frac{C}{4s\pi} \int \frac{d^2 k_\perp}{(2\pi)^2} \frac{N_2}{[k_\perp^4]} \\ &\times g_s^2 g^2 \frac{1}{4} \int \frac{d\alpha_q d^2 q_\perp}{(2\pi)^2} \frac{N_1}{[q_\perp^2 - (\alpha_q + 1)\mu]^2} \frac{1}{(\alpha_q + 1)}. \end{aligned} \quad (3.48)$$

We now compute the two traces, replace β_q , α_k and β_k by their value coming from the three δ -functions and take the limit for s large, i.e. neglect all terms in $1/s$. In order to compute N_1 and N_2 , we use Gribov's trick. We want to compute the two pieces, the pomeron part and the impact factor part, of our diagram separately but both need the contribution of the second to contract the indices in the trace. Hence, we replace each quark/gluon vertex by a quark/gluon eikonal vertex⁵ that consists of replacing γ^ν and γ^μ in the usual vertex by p^ν/\sqrt{s} and p'^μ/\sqrt{s} to simulate the contribution of the lower line in the quark loop and p^ν/\sqrt{s} , p'^μ/\sqrt{s} to simulate the contribution of the upper line in the trace N_2 . We can now compute the traces and we find

$$N_1 \simeq -8s \frac{\alpha_q}{\alpha_q + 1} q_\perp^2, \quad (3.49)$$

$$N_2 \simeq 8s. \quad (3.50)$$

Note that we absorb a factor 4 from the trace in the general factor in front of the amplitude. The imaginary part of the calculated diagram is half the discontinuity that we have just calculated,

⁵This method is inspired by Lech Szymanowski's works and reference [3].

$$\text{Im}(M_{a1}) = g_s^2 \frac{s}{2\pi} \int \frac{d^2 k_\perp}{(2\pi)^2} \frac{1}{[k_\perp^4]} \times g_s^2 g^2 \int \frac{d\alpha_q d^2 q_\perp}{(2\pi)^2} \frac{q_\perp^2}{[q_\perp^2 - (\alpha_q + 1)\mu]^2}, \quad (3.51)$$

this is the first piece of our calculation.

From that, it is easy to compute the diagram with arrows in the opposite direction shown in Fig. 3.11 because it can be obtained by a simple change of variable, $q \rightarrow p + q - k$. The

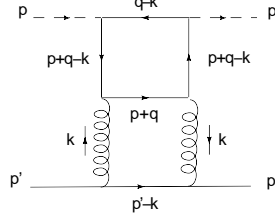


Figure 3.11: Second piece of the amplitude: M_{a2} .

amplitude is thus,

$$M_{a2} = (-ig)_s^2 C \int \frac{d^4 k}{(2\pi)^4} \frac{\text{Tr}[\not{p}' \not{k} \gamma^\nu (\not{p}' - \not{k}) \gamma^\mu]}{[(p' - k)^2 + i\eta][k^2 + i\sigma]^2} \times Q_{a2}(q). \quad (3.52)$$

with $Q_{a2}(q)$ from the quark loop,

$$Q_{a2}(q) = (-1)g_s^2 g^2 \int \frac{d^4 q}{(2\pi)^4} \frac{\text{Tr}[(\not{p} + \not{q} - \not{k}) \gamma^\nu (\not{p} + \not{q}) \gamma^\mu (\not{p} + \not{q} - \not{k}) (\not{q} - \not{k})]}{[(p + q)^2 + i\epsilon][(p + q - k)^2 + i\rho]^2 [(q - k)^2 + i\delta]}. \quad (3.53)$$

By cutting rules we have

$$\begin{aligned} \text{Disc}(M_{a2}) &= -g_s^2 \frac{C}{4s\pi} \int \frac{d^2 k_\perp}{(2\pi)^2} \frac{N_2}{[k_\perp^4]} \\ &\times g_s^2 g^2 \frac{1}{4} \int \frac{d\alpha_q d^2 q_\perp}{(2\pi)^2} \frac{N_1}{[(q_\perp - k_\perp)^2 - (\alpha_q + 1)\alpha_q \mu]^2} \frac{\alpha_q}{(\alpha_q + 1)}, \end{aligned} \quad (3.54)$$

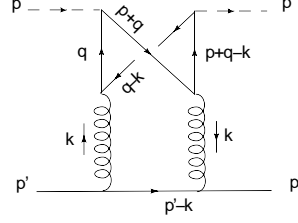
with the two traces in the large- s limit

$$N_1 \simeq -8s \frac{(\alpha_q + 1)}{\alpha_q} (q_\perp - k_\perp)^2, \quad (3.55)$$

$$N_2 \simeq 8s. \quad (3.56)$$

Therefore, the imaginary part of the studied diagram is

$$\text{Im}M_{a2} = g_s^2 \frac{s}{2\pi} \int \frac{d^2 k_\perp}{(2\pi)^2} \frac{1}{[k_\perp^4]} \times g_s^2 g^2 \int \frac{d\alpha_q d^2 q_\perp}{(2\pi)^2} \frac{(q_\perp - k_\perp)^2}{[(\alpha_q + 1)\alpha_q \mu]^2 - (q_\perp - k_\perp)^2}. \quad (3.57)$$

Figure 3.12: Third piece of the amplitude: M_{b1} .**Diagram b**

We now compute the diagram *b* in Fig. 3.12, let us just write the main step. The amplitude is ,

$$M_{b1} = (-ig_s)^2 C \int \frac{d^4 k}{(2\pi)^4} \frac{Tr[p' \gamma^\nu (\not{p}' - \not{k}) \gamma^\mu]}{[(p' - k)^2 + i\eta][k^2 + i\sigma]^2} \times Q_{b1}(q). \quad (3.58)$$

with $Q_{b1}(q)$ the quarks loop,

$$Q_{b1}(q) = (-1)g_s^2 g^2 \int \frac{d^4 q}{(2\pi)^4} \frac{Tr[(\not{p} + \not{q} - \not{k}) \gamma^\nu (\not{p} + \not{q}) \not{q} \gamma^\mu (\not{q} - \not{k})]}{[(p+q)^2 + i\epsilon][(p+q-k)^2 + i\rho][(q-k)^2 + i\delta][q^2 + i\sigma]}. \quad (3.59)$$

By cutting rules we have

$$\begin{aligned} \text{Disc}(M_{b1}) &= -g_s^2 \frac{C}{4s\pi} \int \frac{d^2 k_\perp}{(2\pi)^2} \frac{N_2}{[k_\perp^4]} \\ &\times \frac{g_s^2 g^2}{4} \int \frac{d\alpha_q d^2 q_\perp}{(2\pi)^2} \frac{N_1}{[q^2 - (\alpha_q + 1)\mu][(\alpha_q + 1)\alpha_q \mu - (q_\perp - k_\perp)^2]} \frac{\alpha_q}{(\alpha_q + 1)}, \end{aligned} \quad (3.60)$$

and the two traces in the large- s limit

$$N_1 \simeq -8s(q_\perp^2 - k_\perp \cdot q_\perp), \quad (3.61)$$

$$N_2 \simeq 8s. \quad (3.62)$$

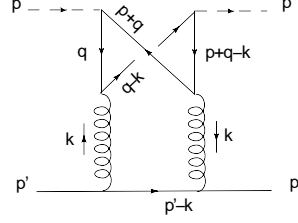
Thus, the imaginary part of the studied diagram is

$$\begin{aligned} \text{Im}(M_{b1}) &= g_s^2 \frac{s}{2\pi} \int \frac{d^2 k_\perp}{(2\pi)^2} \frac{1}{[k_\perp^4]} \\ &\times g_s^2 g^2 \int \frac{d\alpha_q d^2 q_\perp}{(2\pi)^2} \frac{(q_\perp^2 - k_\perp \cdot q_\perp)}{[q^2 - (\alpha_q + 1)\mu][(\alpha_q + 1)\alpha_q \mu - (q_\perp - k_\perp)^2]}. \end{aligned} \quad (3.63)$$

From that and with the change of variable $q \rightarrow p + q - k$, we compute the diagram show in Fig. 3.13. The amplitude is,

$$M_{b2} = (-ig_s)^2 C \int \frac{d^4 k}{(2\pi)^4} \frac{Tr[p' \gamma^\nu (\not{p}' - \not{k}) \gamma^\mu]}{[(p' - k)^2 + i\eta][k^2 + i\sigma]^2} \times Q_{b2}(q). \quad (3.64)$$

with $Q_{b2}(q)$ from the quark-loop,

Figure 3.13: Fourth piece of the amplitude: M_{b2} .

$$Q_{b2}(q) = (-1)g_s^2 g^2 \int \frac{d^4 q}{(2\pi)^4} \frac{\text{Tr}[(\not{p} + \not{q})\gamma^\mu(\not{p} + \not{q} - \not{k})(\not{q} - \not{k})\gamma^\nu(\not{q})]}{[(p+q)^2 + i\epsilon][(p+q-k)^2 + i\rho][(q-k)^2 + i\delta][q^2 + i\sigma]}. \quad (3.65)$$

By cutting rules we have,

$$\begin{aligned} \text{Disc}(M_{b2}) &= -g_s^2 \frac{C}{4s\pi} \int \frac{d^2 k_\perp}{(2\pi)^2} \frac{N_2}{[k_\perp^4]} \\ &\times \frac{g_s^2 g^2}{4} \int \frac{d\alpha_q d^2 q_\perp}{(2\pi)^2} \frac{N_1}{[q^2 - (\alpha_q + 1)\mu][(\alpha_q + 1)\alpha_q \mu - (q_\perp - k_\perp)^2]} \frac{\alpha_q}{(\alpha_q + 1)}, \end{aligned} \quad (3.66)$$

and the two traces in the large- s limit

$$N_1 \simeq -8s(q_\perp^2 - k_\perp \cdot q_\perp), \quad (3.67)$$

$$N_2 \simeq 8s. \quad (3.68)$$

Hence, the imaginary part of the studied diagram is

$$\begin{aligned} \text{Im}(M_{b2}) &= g_s^2 \frac{s}{2\pi} \int \frac{d^2 k_\perp}{(2\pi)^2} \frac{1}{[k_\perp^4]} \\ &\times g_s^2 g^2 \int \frac{d\alpha_q d^2 q_\perp}{(2\pi)^2} \frac{(q_\perp^2 - k_\perp \cdot q_\perp)}{[q^2 - (\alpha_q + 1)\mu][(\alpha_q + 1)\alpha_q \mu - (q_\perp - k_\perp)^2]}. \end{aligned} \quad (3.69)$$

3.3.1 Imaginary part of the amplitude

We now sum the contribution of each diagram to obtain the imaginary part of the amplitude.

$$\begin{aligned} \text{Im}(M_t) &= g_s^2 \frac{s}{2\pi} \int \frac{d^2 k_\perp}{(2\pi)^2} \frac{1}{k_\perp^4} \\ &\times g_s^2 g^2 \int \frac{d\alpha_q d^2 q_\perp}{(2\pi)^2} \left[\frac{2(q_\perp^2 - k_\perp \cdot q_\perp)}{[q^2 - (\alpha_q + 1)\mu][(\alpha_q + 1)\alpha_q \mu - (q_\perp - k_\perp)^2]} \right. \\ &\left. + \frac{q_\perp^2}{[q^2 - (\alpha_q + 1)\mu]} + \frac{(q_\perp - k_\perp)^2}{[(\alpha_q + 1)\alpha_q \mu - (q_\perp - k_\perp)^2]} \right], \end{aligned} \quad (3.70)$$

that can be written as

$$\text{Im}M_t = g_s^2 \frac{s}{2\pi} \int \frac{d^2 k_\perp}{(2\pi)^2} \frac{1}{k_\perp^4} \times \mathcal{F}(k_\perp). \quad (3.71)$$

The amplitude is written in two pieces, one looks like the two-gluon exchange (the simplest pomeron) and the other one $\mathcal{F}(k_\perp)$ can be interpreted as the impact factor of the incoming particle. The impact factor is polynomial in α_q to the fourth noted $P(\alpha_q)$,

$$\mathcal{F}(k_\perp) = g_s^2 g^2 \int \frac{d\alpha_q d^2 q_\perp}{(2\pi)^2} \frac{P(\alpha_q)}{[(\alpha_q + 1)\alpha_q \mu - (q_\perp - k_\perp)^2][q^2 - (\alpha_q + 1)\mu]}, \quad (3.72)$$

with

$$\begin{aligned} P(\alpha_q) = & \alpha_q^4 \mu^2 q_\perp^2 + 2\alpha_q^3 \mu^2 q_\perp \cdot k_\perp \\ & + \alpha_q^2 \mu [2q_\perp^2 (q_\perp \cdot k_\perp - k_\perp^2 - 2\mu) + \mu(k_\perp^2 + 2q_\perp \cdot k_\perp^2)] \\ & + 2\alpha_q [k_\perp^2 (\mu^2 - 2\mu q_\perp \cdot k_\perp - q_\perp^2) + \mu q_\perp \cdot k_\perp (2q_\perp \cdot k_\perp - \mu)] \\ & + [q_\perp^2 (k_\perp^4 - 2k_\perp^2 q_\perp \cdot k_\perp + k_\perp^2 q_\perp^2 - 2\mu q_\perp \cdot k_\perp) \\ & + \mu(k_\perp^2 - 2k_\perp^2 - 2k_\perp^2 q_\perp \cdot k_\perp - 2\mu q_\perp \cdot k_\perp + 4(q_\perp \cdot k_\perp)^2)]. \end{aligned} \quad (3.73)$$

This factor can be integrated in α_q and contributes to the suppression of a k_\perp^2 at the denominator that removes a part of the IR divergence of the amplitude. In the case $\mu = 0$, this means if the incoming particles are massless, the amplitude has the simple form

$$\text{Im}M_t = g_s^2 \frac{s}{2\pi} \int \frac{d^2 k_\perp}{(2\pi)^2} \frac{1}{k_\perp^2} \times g_s^2 g^2 \int \frac{d\alpha_q d^2 q_\perp}{(2\pi)^2} \frac{1}{q_\perp^2 (q_\perp - k_\perp)^2}. \quad (3.74)$$

After integration over α_q between -1 and 0 from the condition (3.38), the imaginary part of the amplitude becomes,

$$\text{Im}(M_t) = g_s^2 \frac{s}{2\pi} \int \frac{d^2 k_\perp}{(2\pi)^2} \frac{1}{k_\perp^2} \times g_s^2 g^2 \int \frac{d^2 q_\perp}{(2\pi)^2} \frac{1}{q_\perp^2 (q_\perp - k_\perp)^2}. \quad (3.75)$$

There is no divergences at large q_\perp^2 . A quark loop in the lower line as in Fig. 3.14 leads to the

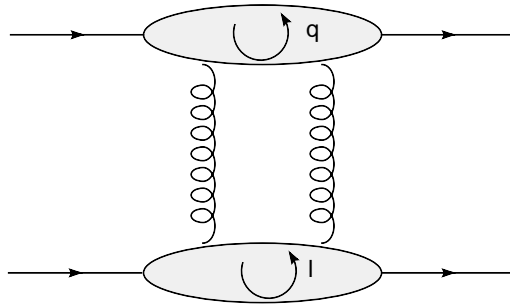


Figure 3.14: Introduction of the two impact factors via a quark loop.

same answer in term of the four-momentum of the loop l and then the amplitude including both impact factor is

$$\text{Im}(M_t) = \frac{s}{2\pi} \int \frac{d^2 k_\perp}{(2\pi)^2} \frac{1}{k_\perp^4} \times \mathcal{F}(k_\perp) \times \mathcal{F}(k_\perp) \quad (3.76)$$

with

$$\mathcal{F}(k_{\perp}) = g_s^2 g^2 \int \frac{d^2 q_{\perp}}{(2\pi)^2} \frac{k_{\perp}^2}{q_{\perp}^2 (q_{\perp} - k_{\perp})^2}, \quad (3.77)$$

The integral diverges at $q_{\perp}^2 = 0$ and $k_{\perp}^2 = q_{\perp}^2$ but because of the large- s limit, we neglected all the $1/s$ terms. Actually, the denominator are

$$\begin{aligned} & [q_{\perp}^2 + \mathcal{O}(1/s)] \\ & [(q_{\perp} - k_{\perp})^2 + \mathcal{O}(1/s)]. \end{aligned} \quad (3.78)$$

Then, the neglected terms lead to a contribution in $\log(s)$ after the last integration over q_{\perp}^2 .

Note that, more physically, this contribution will be cut by confinement effects for real hadrons, as it corresponds to a long-distance effect. However, as we expected the impact factors cancel the divergence in k_{\perp}^2 .

3.4 Outlook

A complete calculation of a physical diffractive cross section for the production of a Higgs bosons will be more complex.

The two incoming particles are proton made of three quarks and with a structure that we have to introduce in the calculation via a wave function. The Higgs is produced via a additional quark loop on the gluon. In order to produce a Higgs boson or another particle in this kind of kinematics, we will need larger longitudinal components for these exchanged gluons to generate the mass of the new particle. Hence the k_{\perp} factorization may not work so well in this case.

Chapter 4

Non-perturbative effects: the Gribov conception

Perturbation theory is a powerful tool in Quantum Electrodynamics and generally in field theory when the coupling constant of the interaction is small, but with Quantum Chromodynamics, the theory of strong interactions, a lot of problems appears. In fact, the coupling of the strong interaction has the particularity of increasing when the distance increases and this leads to a new behavior, color confinement. Because of this strong coupling, the domain of small virtuality cannot be treated with perturbation theory and is affected by what we call non-perturbative effects.

In this chapter, we shall speak about the introduction of non-perturbative effects via a new gluon propagator in a simple calculation. Firstly, we shall describe the physical interest of the shape of this new propagator and, in the second part of the chapter, we shall perform a two-gluon exchange calculation. We shall conclude by a brief study of the answer and of the elements that we have to improve.

4.1 The gluon propagator

In 1978, V.N. Gribov used a new method for the quantization of non-abelian gauge theories [38] and found that we can write the gluon propagator in a new way. This propagator deals with non-perturbative effects and includes them in the calculation. Let us explain the interest of the non-perturbative part inside the propagator and describe its properties.

4.1.1 The Gribov idea

QCD is the theory of strong interactions. The main ingredient are interacting vector bosons and asymptotic freedom¹. This class of theories belongs to a particular group called the non-Abelian gauge theories [28] that are a little bit more complicated to treat than QED and lead to some ambiguity in their definition.

As an example, in QED we can derive propagators of the theory from perturbative calculation but in QCD you cannot do that because higher orders are sensitive to the IR region and then you cannot know the exact propagators of the theory². The quantization problem for non-Abelian gauge theories within the framework of perturbation theory was solved in the

¹A theory where the coupling is strong at small momenta but weak at large momenta.

²Even if it is possible to derive the perturbative propagator from the region of energy where we can apply perturbation theory, the perturbative propagator is different from the exact propagator of QCD.

end of the sixties by Feynman [39], DeWitt [40] and Faddeev and Popov [41]. After these works, most of the calculation in QCD use the gluon propagator

$$D_{\mu\nu}(k^2) = \frac{-ig_{\mu\nu}\delta^{ab}}{k^2 + i\epsilon} \quad (4.1)$$

in the Feynman gauge where a and b are color indices [27]. This propagator is drawn in Fig. 4.1 and has the particularity to diverge at low momentum k but has the expected behavior at large momentum where we can apply perturbation theory. In fact, at large

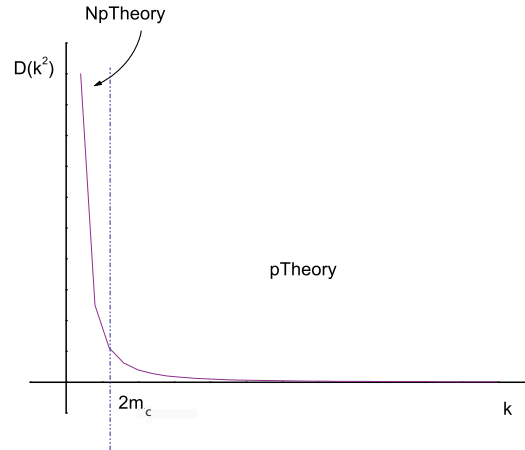


Figure 4.1: Shape of the usual gluon propagator with the limit of validity of the perturbation theory (pTheory).

energy the coupling of QCD becomes smaller and one finds that perturbation theory starts to work perfectly for scales bigger than twice the mass of the charm quark m_c , this means about 3 GeV [42]. However, even if the large-momentum behavior of the gluon propagator is known beyond this limit, we cannot trust the shape of the gluon propagator before. This is because small momenta correspond to long distance physics and poles on the real axis in propagators correspond to real particles that propagate far away in space³. Meanwhile, gluons are always confined so that we cannot trust the propagator and the pole of eq. (4.1). Something must happen in the IR region where non-perturbative effects begin to be important and must be taken into account. According to Gribov, it is possible to improve the quantization of non-Abelian fields through some modifications in the limitation on the integration range in the functional space of non-Abelian fields and this calculation leads to a new possible propagator for the gluon [38],

$$D_{\mu\nu}(k^2) = \frac{-ig_{\mu\nu}\delta^{ab}}{k^2 + \frac{\Lambda^4}{k^2}}. \quad (4.2)$$

The momentum of the gluon is k and Λ is a constant related to the scale of energy where non-perturbative effects begin to appear. This propagator has the shape drawn in Fig. 4.2. It is not divergent but null at $k = 0$ and strongly depends on the parameter Λ at small momentum. We can think that the zero value can be a problem for the physical interpretation but at least it removes the infrared divergence.

³The boson of QED has a similar propagator with a pole at $k = 0$ and we know that photons can propagate onto long distances.

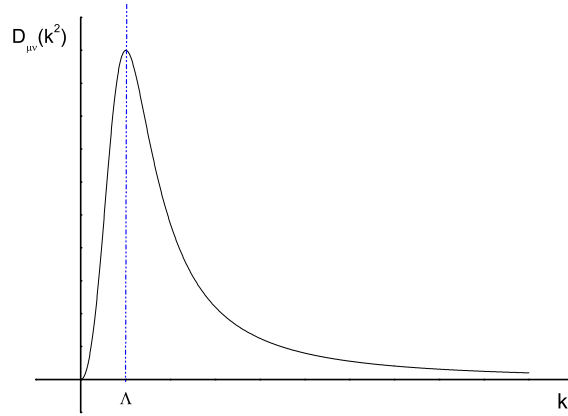


Figure 4.2: Shape of the Gribov propagator.

This propagator includes non-perturbative effects at low momentum via new poles *badly placed*, the Gribov poles, and we can expect a change in the physics at small k . Actually, we could observe consequences of this change at the LHC if this contribution is large enough to influence the amplitude. This means that the new contribution of the Gribov poles must be of order s to be observed and we shall now calculate this contribution for the two-gluon exchange.

4.2 Contribution from the Gribov poles to the pomeron

We now perform the same calculation as in section 3.2.1 but now the new gluon propagator is given by

$$D_{\mu\nu}(k^2) = \frac{-i\delta^{ab}g_{\mu\nu}}{k^2 + \frac{\Lambda^4}{k^2}} = -i\delta^{ab}g_{\mu\nu} \frac{k^2}{(k^2 + i\Lambda^2)(k^2 - i\Lambda^2)}, \quad (4.3)$$

according to eq. (4.2). We will not use the cutting rules because we want to study the position of the new poles in order to understand their contribution. In the second subsection, we compare the answer with the usual calculation for the pomeron and we end by a discussion about the new contribution.

4.2.1 Two-gluon exchange amplitude in the Gribov case

The lowest-order leading Feynman diagrams of the studied process are shown in Fig. 4.3. We

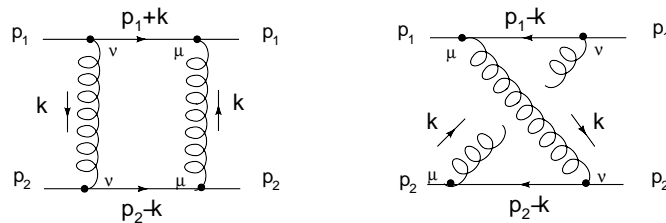


Figure 4.3: The lowest-order leading Feynman diagrams for the two-gluon exchange.

write k in term of the Sudakov variables,

$$k = \alpha p_1 + \beta p_2 + k_\perp, \quad (4.4)$$

using $p_1^2 = p_2^2 = 0$, $p_1 \cdot p_2 = s/2$ and working in the large s limit. The intermediate quarks and incoming particles are supposed to be massless, the coupling constant is g_s and only the gluon propagator is changed from the usual calculation. The direct and crossed amplitude are given by

$$\begin{aligned} A_d &= (-ig_s)^4 C \int \frac{d^4 k}{(2\pi)^4} \frac{\text{Tr}[\not{p}_1 \gamma^\mu (\not{p}_1 + \not{k}) \gamma^\nu] k^2 \text{Tr}[\not{p}_2 \gamma^\nu (\not{p}_2 - \not{k}) \gamma^\mu] k^2}{[(p_1 + k)^2 + i\epsilon][(p_2 - k)^2 + i\eta][(k^2 + i\Lambda^2)(k^2 - i\Lambda^2)]^2} \\ &= g_s^4 \frac{s}{2(2\pi)^2} \int \frac{d\alpha d\beta d^2 k_\perp}{(2\pi)^2} \frac{N_d}{[(\alpha + 1)\beta s + k_\perp^2 + i\epsilon][\alpha(\beta - 1)s + k_\perp^2 + i\eta]P_g^2} \end{aligned} \quad (4.5)$$

$$\begin{aligned} A_c &= (-ig_s)^4 C \int \frac{d^4 k}{(2\pi)^4} \frac{\text{Tr}[\not{p}_1 \gamma^\mu (\not{p}_1 - \not{k}) \gamma^\nu] k^2 \text{Tr}[\not{p}_2 \gamma^\nu (\not{p}_2 - \not{k}) \gamma^\mu] k^2}{[(p_1 - k)^2 + i\epsilon][(p_2 - k)^2 + i\eta][(k^2 + i\Lambda^2)(k^2 - i\Lambda^2)]^2} \\ &= g_s^4 \frac{s}{2(2\pi)^2} \int \frac{d\alpha d\beta d^2 k_\perp}{(2\pi)^2} \frac{N_c}{[(\alpha - 1)\beta s + k_\perp^2 + i\epsilon][\alpha(\beta - 1)s + k_\perp^2 + i\eta]P_g^2}. \end{aligned} \quad (4.6)$$

N_d and N_c are the traces in Sudakov variables and C is the color factor equals to $2/9$ as in the usual calculation. The denominator of the gluon propagator is given by

$$P_g = [(\alpha\beta s + k_\perp^2 + i\Lambda^2)(\alpha\beta s + k_\perp^2 - i\Lambda^2)]. \quad (4.7)$$

We now only consider the direct amplitude but it is clear that the method is identical for the crossed diagram. The direct integrand has four poles, two of them are the usual poles coming from the quark propagators,

$$\beta_1 = \frac{-k_\perp^2 - i\epsilon}{(\alpha - 1)s}, \quad (4.8)$$

$$\beta_2 = \frac{-k_\perp^2 - i\eta}{\alpha s} + 1, \quad (4.9)$$

and the new gluon propagator has two double poles at

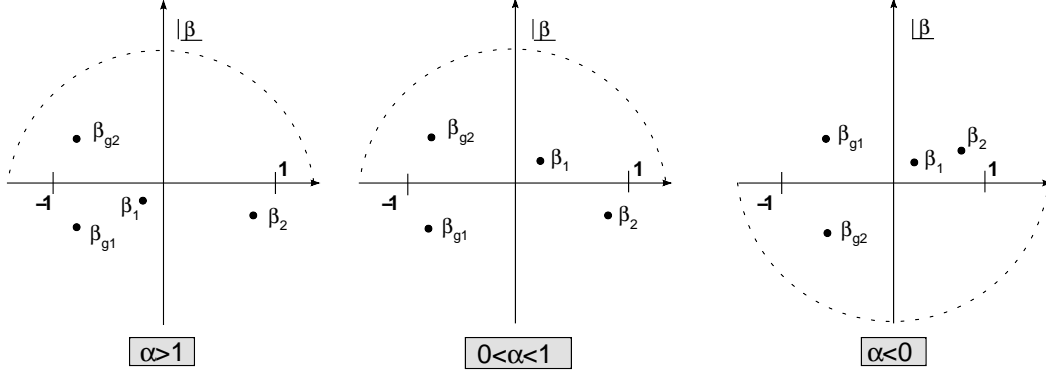
$$\beta_{g1} = \frac{-k_\perp^2 - i\Lambda^2}{\alpha s}, \quad (4.10)$$

$$\beta_{g2} = \frac{-k_\perp^2 + i\Lambda^2}{\alpha s}. \quad (4.11)$$

Their positions in function of the value of α is shown in Fig. 4.4. We immediately note that we have to deal with a new pole β_{g2} inside the integration contour. Via the Cauchy theorem for double poles and noting Res_{β_i} the residue in β_i , we obtain the integral on β

$$I_\beta = 2i\pi \left[\int_0^1 \text{Res}_{\beta_1} d\alpha + \int_1^\infty \text{Res}_{\beta_{g2}} d\alpha - \int_{-\infty}^0 \text{Res}_{\beta_{g2}} d\alpha \right], \quad (4.12)$$

the integral on the half circle vanishes because the integrand decreases faster than $1/\beta^2$. The last term of eq. (4.12) leads to the usual contribution of the usual pole in the amplitude but the sum of the two first terms is the new contribution from the Gribov poles. We keep the

Figure 4.4: The position of the poles in the β -integral.

usual answer for the end of the calculation and just care about the Gribov contribution that we note with an index g . The direct diagram gives us

$$I_{dg} = 2i\pi \int_0^\infty [\text{Res}_{\beta_{g2}}(\alpha) - \text{Res}_{\beta_{g2}}(-\alpha)]d\alpha. \quad (4.13)$$

The symmetry of the integrand leads to a result that can be written as a function of α^2 and if we rename $\alpha^2 = x$,

$$\begin{aligned} I_{dg} &= 2i\pi \int_0^\infty f(\alpha^2)d\alpha^2 \\ &= 2i\pi \int_0^\infty f(x)dx. \end{aligned} \quad (4.14)$$

The result for the crossed diagram leads to the same structure of the α -integral and if we note I_g the sum of the direct and crossed integrand, we find that we have to compute

$$I_g = \frac{i\pi}{9\Lambda^2}C \int_0^\infty dx \frac{P(x)}{[(k_\perp^2 + (x-1)i\Lambda^2)(k_\perp^2 - (x-1)i\Lambda^2)][(-\Lambda^4 - xs^2)^2]}, \quad (4.15)$$

with

$$\begin{aligned} P(x) &= [(\Lambda^8 + k_\perp^4 \Lambda^4)s^2 x^2 \\ &\quad + (3k_\perp^4 \Lambda^8 - \Lambda^{12} - \Lambda^8 s^2 - 4ik_\perp^2 \Lambda^6 s^2 + 2k_\perp^4 \Lambda^4 s^2 - k_\perp^8 s^2)x \\ &\quad + (\Lambda^8 - 2k_\perp^4 \Lambda^4 - 4ik_\perp^6 \Lambda^2 + k_\perp^8)\Lambda^4]. \end{aligned} \quad (4.16)$$

The new integrand has no poles in the domain of integration and then we can perform the integral on x directly. In the large- s limit, we obtain

$$\begin{aligned} \mathcal{M}_g^s &= \frac{g_s^4}{4\pi}C \int \frac{d^2 k_\perp}{(2\pi)^2} \frac{N_g}{(i\Lambda^2 - k_\perp^2)^3 \Lambda^4} \\ N_g &= [2\log(i) - 2\log(s) - 4\log(\Lambda^2) - 2\log(k_\perp^2 - i\Lambda^2)](-i\Lambda^6 + 3k_\perp^2 \Lambda^4 - ik_\perp^4 \Lambda^2 - k_\perp^6) \\ &\quad + 2(k_\perp^4 - \Lambda^4)(i\Lambda^2 - 2k_\perp^2). \end{aligned} \quad (4.17)$$

We have a divergence of the integral over k_{\perp} at infinity which may get regulated by the introduction of an impact factor.

We now have the contribution \mathcal{M}_g of the Gribov poles to the total amplitude for two-gluon exchange and the bad news is that it is not of order s . This means that it misses a factor 10^8 in order to have any influence upon the physics at the LHC. However, we will make a brief study of this result.

4.2.2 Properties of the new contribution

Let us now show some graphics of the different pieces of the amplitude and compare it with the usual amplitude for two-gluon exchange.

First, we write the Gribov contribution to the amplitude in term of its real part and its imaginary part in the large- s limit,

$$\mathcal{M}_g^s = \frac{g_s^4}{4\pi} C \int \frac{d^2 k_{\perp}}{(2\pi)^2} [\text{Re}\mathcal{M}_g^s + i\text{Im}\mathcal{M}_g^s], \quad (4.18)$$

with

$$\begin{aligned} \text{Re}\mathcal{M}_g^s &= -\pi \frac{N_{Reg}}{(k_{\perp}^2 + i\Lambda^2)^3 (k_{\perp}^2 - i\Lambda^2)^3 \Lambda^2} \\ N_{Reg} &= [4(2\log(\Lambda^2) - \log(s)) \\ &\quad - \log[(k_{\perp}^2 + i\Lambda^2)(k_{\perp}^2 - i\Lambda^2)]] (k_{\perp}^8 - 8k_{\perp}^4 \Lambda^4 - \Lambda^8) (k_{\perp}^2 + \Lambda^2) (k_{\perp}^2 - \Lambda^2) \\ &\quad + 4[2k_{\perp}^{12} + 2k_{\perp}^{10} \Lambda^2 \pi - 5k_{\perp}^8 \Lambda^4 - 6k_{\perp}^6 \Lambda^6 \pi + 2k_{\perp}^4 \Lambda^8 + \Lambda^{12} \\ &\quad - 2(k_{\perp}^4 - 3\Lambda^4) \tan^{-1}\left(\frac{\Lambda^4}{k_{\perp}^2}\right) k_{\perp}^6 \Lambda^2]. \end{aligned} \quad (4.19)$$

The imaginary part is given by

$$\begin{aligned} \text{Im}\mathcal{M}_g^s &= -2\pi \frac{N_{Img}}{(k_{\perp}^2 + i\Lambda^2)^3 (k_{\perp}^2 - i\Lambda^2)^3 \Lambda^2} \\ N_{Img} &= 2[4(2\log(\Lambda^2) - \log(s)) - \log[(k_{\perp}^2 + i\Lambda^2)(k_{\perp}^2 - i\Lambda^2)]] (k_{\perp}^4 - 3\Lambda^4) k_{\perp}^6 \Lambda^4 \\ &\quad - [k_{\perp}^8 \pi - 10k_{\perp}^6 \Lambda^2 - 8k_{\perp}^4 \Lambda^4 \pi - 2k_{\perp}^2 \Lambda^6 - \Lambda^8 \pi] (k_{\perp}^2 + \Lambda^2) (k_{\perp}^2 - \Lambda^2) \\ &\quad + (k_{\perp}^8 - 8k_{\perp}^4 \Lambda^4 - \Lambda^8) (k_{\perp}^2 + \Lambda^2) (k_{\perp}^2 - \Lambda^2) \tan^{-1}\left(\frac{\Lambda^4}{k_{\perp}^2}\right). \end{aligned} \quad (4.20)$$

We set $s=100 \text{ GeV}^2$ in order to be in the domain of energies where the pomeron begins to be a large contribution to the amplitude. We choose a value for Λ equal to 1 GeV because this parameter is related to the energy scale of non-perturbative physics as we explain in Section 4.1.1. Non-perturbative effects introduced through the Gribov propagator are supposed to occur at small momenta and the contribution of Gribov poles is important when

$$\frac{\Lambda^4}{k^2} \ll k^2. \quad (4.21)$$

Usually one thinks that non-perturbative effects take place below the mass of the proton hence we can set $\Lambda=1$ GeV or smaller. We draw both the imaginary part and the real part of the amplitude in Fig. 4.5. First, we do not have a good behavior in k_{\perp} , the real part diverges

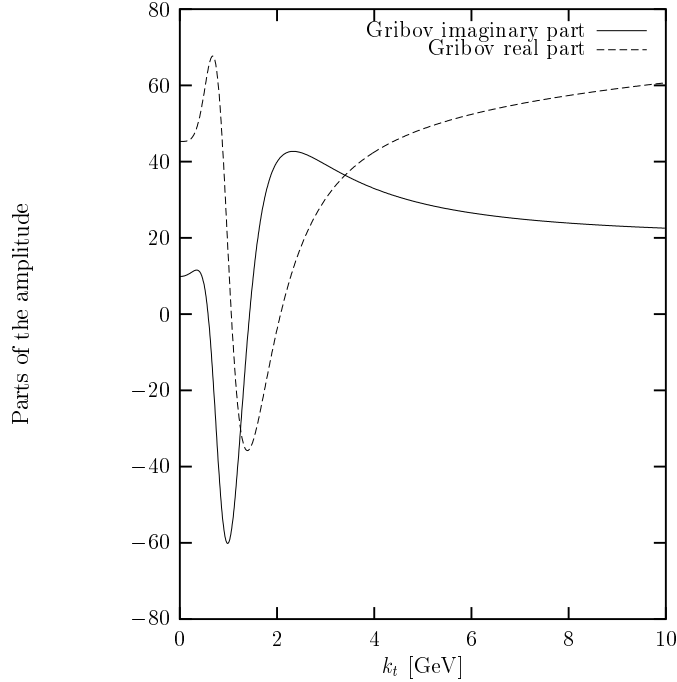


Figure 4.5: Real part and imaginary part of the Gribov contribution in function of k_{\perp} . We have set $s=100$ GeV² and $\Lambda=1$ GeV.

and the imaginary part quickly becomes a constant. Another note is that the Gribov real and imaginary contribution goes through zero and is minimum at $k_{\perp} = \Lambda$. Actually, the divergence of the real and imaginary parts can be explained by the fact that we have no impact factor in the calculation, we should improve this behavior via the introduction of a quark loop that shall constrain the β parameter and force k_{\perp} to be below the inverse radius of the incoming particles. The second point is the order of this contribution. We expected an s factor before the last integral but actually, we can show that the leading term in s of the direct diagram exactly cancels with the leading term in s of the cross diagram and then after the sum, only the sub-leading terms survive.

We now compare the Gribov contribution to the usual contribution given by

$$I = ig^4 s C \int_0^s \frac{d^2 k_{\perp}}{(2\pi)^2} \left[\frac{k^2}{(k^2 + i\Lambda^2)(k^2 - i\Lambda^2)} \right]^2. \quad (4.22)$$

as we calculated⁴ in section 3.2.1. In the next graph, Fig. 4.6, we draw the contribution of the Gribov poles to the imaginary part and the usual pole contribution from eq. (4.22). The last graph, Fig. 4.7, is the total Gribov imaginary part of the amplitude (Gribov poles contribution+usual poles contribution) compared with the contribution of the old propagator for the two-gluon exchange. The Gribov contribution is indeed very small in the domain of interest, i.e. below 1 GeV and cannot change the physics for the studied process. All the

⁴This answer was found via the same methods: study of the poles and integration by residue. All the REDUCE program are in Appendix C.2.

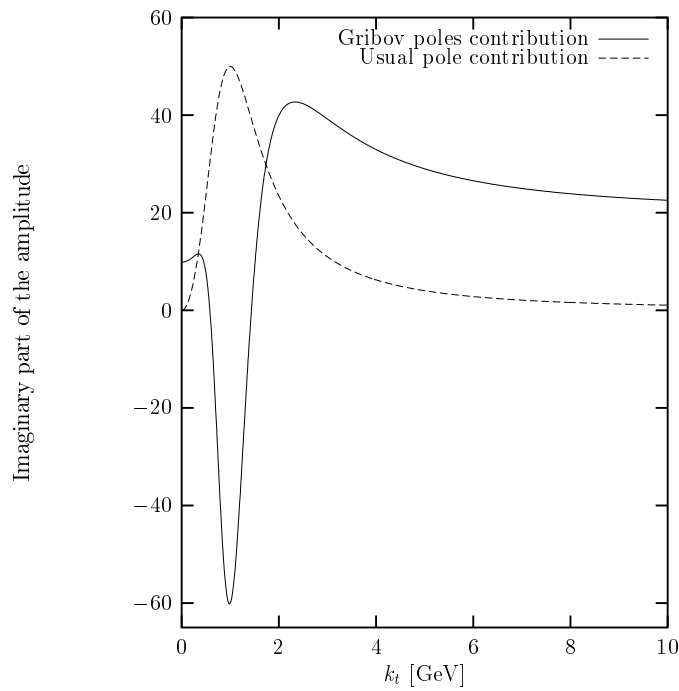


Figure 4.6: Contribution of the Gribov poles to the imaginary part and the usual contribution from eq. (4.22).

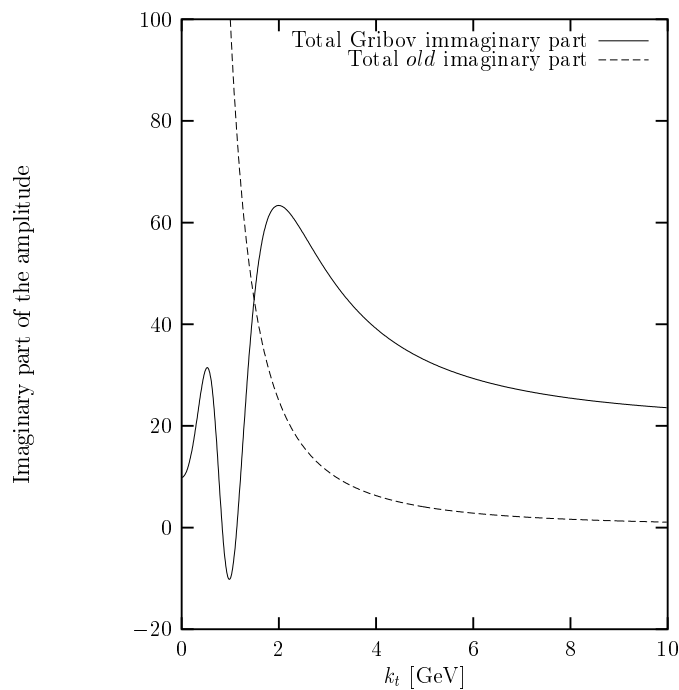


Figure 4.7: Total contribution of Gribov propagator to the imaginary part of the amplitude (Gribov poles contribution+usual poles contribution) compared with the contribution of the old propagator for the two-gluon exchange.

values beyond 1 GeV cannot be trusted because they have to be cut by an impact factor.

Hence, the Gribov contribution is subleading in s and the divergence of the k_{\perp} integral must be removed via the introduction of a quark loop.

Symmetry property of diagrams in the large s limit.

As an exercise, we have also checked crossing symmetry of the amplitude: the crossed diagram must be equal to the direct diagram where we change s into $-s$.

This property is easy to understand with the help of the diagrams drawn in Fig. 4.8. In the

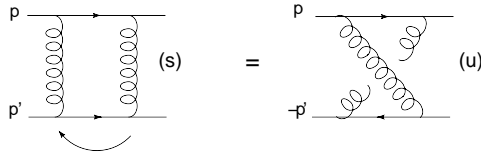


Figure 4.8: Symmetry in the two-gluon exchange.

first diagram we have

$$s = (p + p')^2. \quad (4.23)$$

We obtain the second diagram by a flip of the lower line and this flip corresponds to change the channel $s \rightarrow u$, this is obvious from the definition of u and of the Mandestam variables,

$$\begin{aligned} u &= 4m^2 - t - s \\ &= -s, \end{aligned} \quad (4.24)$$

in the large- s limit and at zero momentum transfer ($t=0$). Hence, the subtraction of the crossed diagram in $-s$ from the direct diagram in s must be zero. Thus, we write a REDUCE program that adds the direct and crossed diagram after each steps of the calculation and show it in Appendix C.3.1. It appears that this property is true in our calculation and tells us that the extraction of real and imaginary parts is correct.

4.3 Conclusion and outlook

In this chapter, we explored the possibility of introducing non-perturbative effects via the Gribov gluon propagator in the calculation of the amplitude for a given process. We described the property of this new propagator and performed a calculation of the two-gluon exchange amplitude in this particular case.

Up to now, we show that the Gribov contribution is subleading in s . We could make some improvement with a quark loop in order to remove the divergence in k_{\perp} and study exactly how this contribution influences the amplitude. If the effects cannot be shown at the LHC, it could be interesting to explore their importance at lower energies, and particularly the contribution to the real part.

Conclusion

In this work, we have introduced the basic tools needed to study diffraction in high-energy physics. We defined the diffractive processes and explained their interest in the detection of particles but also the interest of diffraction as a QCD laboratory, a field to test the theory and a discovery channel for the Higgs boson. In the second chapter, we introduced our tools. Cutting rules that allow us to calculate directly the imaginary part of a Feynman diagram and the Optical theorem or the dispersion relations that relate this imaginary part to the total amplitude and measurable quantities as the cross section. We illustrate this chapter by a simple calculation using all the tools and variables introduced previously. From that, we understood that a main ingredient of diffractive and high-energy physics is the pomeron. This was the topic of the third chapter. The exact nature of the pomeron is not known and we shown that the BFKL description or the Regge approach have some problems to describe this trajectory. The lack of sound theory let us think that QCD has yet interesting problems to solve.

After that, we presented the first calculation in this work. From the previous chapter, we think that diffractive production is a possible way of production of the Higgs boson but complete models for it are complex. Hence, we want to develop a simple method of calculation that we shall complicate in later studies. We divide our calculation in pieces and calculate the first step, a two-gluon exchange between two quark loops. The results was interesting because it removed the divergence in the IR region and enabled us to interpreted physically the different pieces of the calculation, the impact factor and the usual two-gluon exchange. The calculation can lead to the diffractive production of a Higgs boson via some improvement, the addition of a quark loop in the kinematics of the gluon, the introduction of momentum transfer $\Delta \neq 0$ in order to obtain longitudinal momentum to produce the mass of the Higgs.

The second calculation was the introduction of non-perturbative effects in a known amplitude via a new gluon propagator introduced by Gribov. This propagator includes a parameter Λ related to the scale of energy at which non-perturbative effects begin to appear. This study was preliminary and needs improvements. Firstly, we have to introduce the impact factor in the upper and lower fermions lines to remove the divergence in k_{\perp} and study the importance of the value of Λ in the model. Secondly, it will be interesting to study the real part of the diagram because, as we shown, this part is important and can change details of the physics. This calculation also needs a more detailed study of the different steps and a complete comprehension of the influence of the transverse momentum.

Appendix A

Integration by residue

Most of the integrals of this work are performed by residue theorem. The method of integration comes from the Cauchy theorem of integration on a closed curve.

A.1 Residue theorem

Residue theorem 1 *If $f(z)$ is an analytic and uniform function inside and on a closed contour \mathcal{C} except at a finite number of singularities z_1, \dots, z_n inside \mathcal{C} , then*

$$\oint_{\mathcal{C}} f(z) dz = 2i\pi \sum_{m=1}^n \text{Res}_{z_m}[f(z)],$$

with $\text{Res}_{z_m}[f(z)]$ the residue of $f(z)$ in the pole z_m , with \mathcal{C} is the curve show in Fig. A.1.

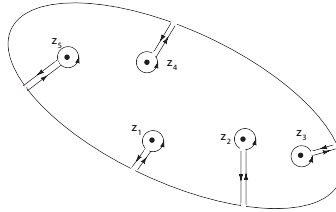


Figure A.1: Closed contour defines by the Cauchy theorem.

The definition of the residue depends of the multiplicity of the poles z_m for a given function $f(z)$.

1. Simple pole: $\text{Res}_{z_m}[f(z)] = \lim_{z \rightarrow z_m} (z - z_m) f(z)$.
2. Pole of order α : $\text{Res}_{z_m}[f(z)] = \frac{1}{(n-1)!} \lim_{z \rightarrow z_m} \frac{d^{\alpha-1}}{dz^{\alpha-1}} (z - z_m)^\alpha f(z)$.

In practice, we shall integrate on a closed contour in a half-complex plane that will be always similar to the one in Fig. A.2. The integral in the total contour \mathcal{C} is divided in integrals on the different pieces,

$$\oint_{\mathcal{C}} f(z) dz = \int_{\mathcal{C}_\infty} f(z) dz + \int_{\mathcal{C}_\epsilon} f(z) dz + \int_{\mathcal{C}_{\eta_1}} f(z) dz + \int_{\mathcal{C}_{\eta_2}} f(z) dz + \int_{\mathcal{C}_R} f(z) dz, \quad (\text{A.1})$$

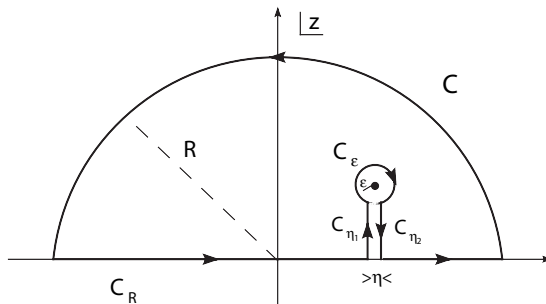


Figure A.2: Closed contour.

where C_∞ is the big half semicircle and C_ϵ the little one around the pole. The contribution of $C_{\eta1}$ and $C_{\eta2}$ are exactly the same but with an opposite sign and their sum always leads to zero as $\eta \rightarrow 0$. The integration on C_R is equivalent to the principal part of an integration along the real axis,

$$p \int_{-\infty}^{\infty} \frac{f(z)}{z - z_m} dz = \lim_{\epsilon \rightarrow 0} \left[\int_{-\infty}^{z_0 - \epsilon} + \int_{z_0 + \epsilon}^{\infty} \right] \frac{f(z)}{z - z_0} dz, \tag{A.2}$$

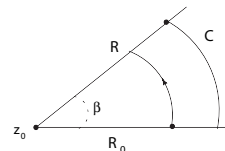
where z_0 are the position of the pole z_m on the real axis. Then we have to compute the contribution of C_∞ and C_ϵ that is the contribution of the pole to the integral. However, the contribution from the big contour is usually zero when the contour goes to infinity. Mathematically, if $R \rightarrow \infty$ the contribution from $\int_{C_\infty} f(z) dz \rightarrow 0$ through the Estimation lemma.

Estimation lemma 1 *If C_∞ is an arc of center z_0 and of radius R intercepted by an oriented angle β , $f(z)$ a continuous function in the closed sector $|z - z_0| \geq R_0$ and such as*

$$\lim_{z \rightarrow \infty} (z - z_0) f(z) = L,$$

with $L \in \mathbb{C}$. Then

$$\lim_{R \rightarrow \infty} \int_{C_\infty} f(z) dz = iL\beta$$



We immediately see that this limit is zero if the function $f(z)$ decreases faster than $1/z$.

Appendix B

Feynman rules

Let us remind the reader of the Feynman rules for the theories used in this work. In both of them:

- Momentum is conserved at each vertex.
- Undetermined loop momenta are integrated over $\int \frac{d^4 p}{(2\pi)^4}$.
- Fermion loops are multiplied by -1

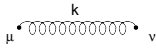
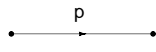
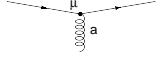
All the rule are in written in the Feynman gauge.

B.1 Feynman rules for QCD

The gauge invariant lagrangian for QCD is

$$\mathcal{L} = \bar{q}(i\gamma^\mu \delta_\mu - m)q - g(\bar{q}\gamma^\mu T_a q)A_\mu^a - \frac{1}{4}G_{\mu\nu}^a G_a^{\mu\nu}. \quad (\text{B.1})$$

Feynman rules for QCD:

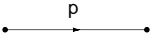

Diagram	Rule
	$\frac{-ig_{\mu\nu}\delta_{ab}}{k^2+i\epsilon}$
	$\frac{i(\not{p}+m)}{p^2-m_q^2+i\epsilon}$
	$-ig_s\gamma^\mu \frac{\lambda_a}{2}$

B.2 Feynman rules for ϕ^3 theory

The gauge invariant lagrangian for ϕ^3 theory is

$$\mathcal{L} = \frac{1}{2}(\delta_\mu\phi)^2 - \frac{m}{2}\phi^2 - \frac{\lambda}{3!}\phi^3. \quad (\text{B.2})$$

Feynman rules for ϕ^3 theory:

Diagram	Rule
	$\frac{i}{p^2 - m_q^2 + i\epsilon}$
	$-i\lambda$

Appendix C

REDUCE programs

In this section of the appendix, we show the REDUCE programs that were used during our work. Most of the programs has the same structure:

1. A common part with the definition of variables, vectors and the trace in the numerator.
2. The complete calculation of the amplitude with poles, residues and integration.
3. The amplitude calculation by cutting rules.

C.1 One loop diagram in Sudakov variables

```

→ONE LOOP DIAGRAM in SUDAKOV VARIABLES

→Definition of vectors and variables
vector p1,p2,p;
vector q,qt;
Svertex:=-ima*g;
mq:=0;
→Definition of the scalar products
let p1.p1=0;
let p2.p2=0;
let p1.p2=s/2;
→Change of variables
p:=p1+m/s*p2;
q:=aq*p1+bq/s*p2+qt;
jacq:=1/2;
let p1.qt=0;
let p2.qt=0;
→Numerator
n:=(-1)*[Svertex*(g(l1,p+q)+mq)*Svertex*(g(l2,-p+q)+mq)];
index mu,nu;
n:=8*n;
→Propagators denominators
Pq:=(p+q).(p+q)-mq**2+ima*epsi;
Pq1:=(-p+q).(-p+q)-mq**2+ima*epsi;

→COMPLETE CALCULATION
→Study of the integral if bq=m or bq=-m
bq:=-m;
Int:=[n]/[Pq*Pq1];
solve(den(Int),aq);
→Poles for aq
solve(Pq,aq);
aq1:=part(ws,1,2);
solve(Pq1,aq);
aq2:=part(ws,1,2);
epsi:=0;
→Residue1
aq-aq1;
resa:=[2*ima*Pi]/[Pq1*(bq+m)];
dresa:=sub(aq=aq1,den(resa));
nresa:=sub(aq=aq1,n);
→pole for bq
Pq1:=-dresa+ima*eta;
n:=nresa;
solve(Pq1,bq);
bq1:=part(ws,2,2);
eta:=0;
→Residue2
bq-bq1;
resb:=-1*-1*[2*ima*Pi]/[bq-sqrt(m**2+m*qt.qt)];
dresb:=sub(bq=bq1,den(resb));
nresb:=sub(bq=bq1,nresa);
→Amplitude
ampl:=[nresb*jacq*jacp]/[dresb*(2*Pi)**4];
end;

→By CUTTING RULES
epsi:=0;
eta:=0;
→Cut
c1:=solve(pq,aq);
aq:=part(ws,1,2);
c2:=solve(pq1,bq);
bq:=part(ws,2,2);
→Amplitude
amplc:=ima*[n*jacp*jacq]/[(2*Pi)**4*(bq-sqrt(m**2+m*qt.qt))];
end;

```


C.2 Two gluon exchange

```

→TWO-GLUON EXCHANGE

→Definition of vectors and variables
vector p1,p2;
vector k,kt;
Gvertex:=-ima*gs;
→Definition of the scalar products
let p1.p1=0;
let p2.p2=0;
let p1.p2=s/2;
→Change of variables
k:=ak*p1+bk*p2+kt;
jac:=s/2;
let p1.kt=0;
let p2.kt=0;
%m:=0;
→Propagators
Pr1:=(p1-k).(p1-k)-m**2+ima*epsi;
Pg1:=k.k+ima*epsi;
Pg2:=k.k+ima*epsi;
Pr3:=(p2+k).(p2+k)-m**2+ima*epsi;
Pr3c:=(p2-k).(p2-k)-m**2+ima*epsi;
→Poles
solve(Pr1,bk);
bk1:=part(ws,1,2);
solve(Pr3,bk);
bk3:=part(ws,1,2);
solve(Pr3c,bk);
bk3c:=part(ws,1,2);
solve(Pg,bk);
bk2:=part(ws,1,2);
epsi:=0;
→Numerator
ft:=8;
nint:=[Gvertex*g(l1,p1,mu,p1,nu)*Gvertex
*g(l2,p2,nu,p2,mu)*Gvertex*Gvertex]*1/s**2;
nintc:=[Gvertex*g(l1,p1,nu,p1,mu)
*Gvertex*g(l2,p2,mu,p2,nu)*Gvertex*Gvertex]*1/s**2;
index mu,nu;
nint;
nintc;
→Residue
%res:=[int*(bk-bk1)];
%res;
dint:=Pg1*Pg2*Pr3;
dintc:=Pg1*Pg2*Pr3c;
re:=[nint]/[(s*(ak-1))*dint];
rec:=[nintc]/[(s*(ak-1))*dintc];
re;
intn:=-2*ima*Pi*re;
rec;
intnc:=-2*ima*Pi*rec;
bk:=bk1; →Amplitude
intn;
intnc;
inta:=jac*ft*(intn+intnc);
let kt.kt=ktt;
on factor;
inta;
Suite and integration: ampl.red
end;

```

```

→SUITE POM.RED
→Integration over alpha
  intn:=(- 8*(ak**2*kt**2 - 3*ak**2 *m**2-2*ak*kt**2
    +4*ak*m**2 +2*kt**2-2*m**2)*
    (ak - 1)**2*gs**4 *ima*pi*s**2)/((ak**2*s - ak*s + kt**2 - m**2)*
    (ak**2*s - ak*s - kt**2+ m**2)*(ak*m**2 - kt**2)**2);
  %m:=0;
  intn2:=sub(ak=(ak/s),intn);
  jaca:=1/s;
  intn2:=intn2*jaca;
  Sintn:=lterm(num(intn2),s)/lterm(den(intn2),s);
  Sintn;
  inta:=int(Sintn,ak);
  ao:=sub(ak=0,inta);
  ai:=sub(ak=1,inta);
  Ampl:=ai-ao;
  Amplg;
→Leading term
  Sampl:=lterm(num(ampl),s)/lterm(den(ampl),s);
  Sampl;
end;

```

C.3 Gribov contribution

```

→GRIBOV PROPAGATOR
→Addition of the Gribov contribution

→Definition of vectors and variables
vector p1,p2;
vector k,kt;
Gvertex:=-ima*gs;
→Definition of the scalar products
let p1.p1=0;
let p2.p2=0;
let p1.p2=s/2;
→Change of variables
k:=ak*p1+bk*p2+kt;
jac:=s/2;
let p1.kt=0;
let p2.kt=0;
m:=0;
→Propagators
Pr1:=(p1-k).(p1-k)-m**2+i*epsi;
Pr2a:=(kt.kt+ak*bk*s+ima*(la**2))**2;
Pr2b:=(kt.kt+ak*bk*s-ima*(la**2))**2;
Pr3:=(p2+k).(p2+k)-m**2+i*epsi;
Pr3c:=(p2-k).(p2-k)-m**2+i*epsi;
→Poles
dint:=Pr1*Pr3;
dintc:=Pr1*Pr2*Pr3c*Pr4;
solve(Pr1,bk);
%bk1:=part(ws,1,2);
solve(Pr3,bk);
%bk2:=part(ws,1,2);
solve(Pr3c,bk);
%bk2c:=part(ws,1,2);
gr:=solve(Pr2,bk);
bk3:=part(gr,1,2);
bk4:=part(gr,2,2);
epsi:=0;
bk3:=(-kt.kt+ima*(la**2))/(ak*s);
→Numerator
ft:=2/9;
nint:=[Gvertex*g(l1,p1,mu,p1-k,nu)*Gvertex*g(l2,p2,nu,p2+k,mu)*Gvertex*Gvertex];
nintc:=[Gvertex*g(l1,p1,nu,p1-k,mu)*Gvertex*g(l2,p2,mu,p2-k,nu)*Gvertex*Gvertex];
index mu,nu;
nint;
nintc;
→Residue
%res:=df[int*(bk-bk3)**2];
%res;
Pr1:=(p1-k).(p1-k)-m**2;
Pr3:=(p2+k).(p2+k)-m**2;
Pr3c:=(p2-k).(p2-k)-m**2;
dint:=Pr1*Pr3;
dintc:=Pr1*Pr3c;
re:=[nint*((kt.kt+ak*bk*s)**2)]/(((ak*s)**2)*dint*pr2a];
rec:=[nintc*((kt.kt+ak*bk*s)**2)]/(((ak*s)**2)*dintc*pr2a];
re;
res:=-df(re,bk);
rec;
resc:=-df(rec,bk);
bk:=bk3;
res;
intg:=2*ima*Pi*[sub(ak=akk,res)-sub(ak=-akk,res)];
resc;
intgc:=2*ima*Pi*[sub(ak=akk,resc)-sub(ak=-akk,resc)];
→Amplitude
intg;
intgc;
amplg:=jac*ft*(intg+intgc);
amplg:=amplg/(2*akk);
let akk**2=x;
let kt.kt=ktt;
let la**2=l;
on factor;
amplg;
%Suite and integration: amplg.red
end;

```

→RESULTS of POMG.RED

```

intg :=(2*(ima**6 *1**6*x-ima**6*1**6+ 3*ima**4*kt**4 *1**4*x
-2*ima**4*kt**4*1**4+ima**4*1**4*s**2*x**2-ima**4*1**4*s**2*x
+4*ima**3*kt**6*1**3+4*ima**3*kt**2*1**3*s**2*x-ima**2*kt**8 *1**2
-ima**2*kt**4*1**2*s**2*x**2- 2*ima**2*kt**4*1**2 *s**2*x
-kt**8 *s**2 *x)*gs**4 *ima**4 *pi*s**2 )/((ima**2*1**2*x
-ima**2 *1**2 +2*ima*kt**2*1-kt**4)**2
*(ima**2 *1**2- s**2 *x)**2 *1);

```

intg;

inta:=int(intg,x);

ao:=sub(x=0,inta);

x:=1/y;

inta;

let log((ima**2 *1**2 *y-s**2)/y)=log(ima**2 *1**2 *y-s**2)-log(y);

let log((-ima**2 *1**2 *y+ima**2 *1**2+2*ima*kt**2 *1*y-kt**4*y)/y)

=log(-ima**2 *1**2 *y+ima**2 *1**2+2*ima*kt**2*1*y-kt**4*y)-log(y);

inta;

ai:=sub(y=0,inta);

Amplg:=ai-ao;

Amplg;

let log(-(s**2))=log(-1)+2log(s);

let log(-(1**2))=log(-1)+2log(1);

Amplg:=Amplg;

→Leading term

Samplg:=lterm(num(amplg),s)/lterm(den(amplg),s);

Samplg;

let log(-s**2)=log(-1)+2log(s);

samplg;

→Leading-log

Lamplg:=lterm(num(samplg),log(s))/lterm(den(samplg),log(s));

Lamplg;

end;

C.3.1 Symmetry property of diagram in the large s limit

```

→AMPL VERSUS AMPLGC
→Check step by step of the symmetry s/-s

→Definition of vectors and variables
vector p1,p2;
vector k,kt;
Gvertex:=-ima*gs;
let p1.p1=0;
let p2.p2=0;
let p1.p2=s/2;
→Change of variables
k:=ak*p1+bk*p2+kt;
jac:=s/2;
let p1.kt=0;
let p2.kt=0;
m:=0;
→Direct and cross amplitude
ft:=8;
nint:=[Gvertex*g(l1,p1,mu,p1-k,mu)*Gvertex*g(l2,p2,mu,p2+k,mu)*Gvertex*Gvertex];
nintc:=[Gvertex*g(l1,p1,mu,p1-k,mu)*Gvertex*g(l2,p2,mu,p2-k,mu)*Gvertex*Gvertex];
index mu,mu;
nint;
nintc;

Pr1:=(p1-k).(p1-k)-m**2;
Pr3:=(p2+k).(p2+k)-m**2;
Pr3c:=(p2-k).(p2-k)-m**2;
Pr2a:=(kt.kt+ak*bk*s+ima*(la**2))**2;
Pr2b:=(kt.kt+ak*bk*s-ima*(la**2))**2;

dint:=Pr1*Pr3;
dintc:=Pr1*Pr3c;
re:=[nint*((kt.kt+ak*bk*s)**2)]/[(ak*s)**2]*dint*pr2a];
rec:=[nintc*((kt.kt+ak*bk*s)**2)]/[(ak*s)**2]*dintc*pr2a];
re;
res:=-df(re,bk);
rec;
resc:=-df(rec,bk);
bk3:=(-kt.kt+ima*(la**2))/(ak*s);
bk:=bk3;
res;
intg:=2*ima*Pi*[sub(ak=akk,res)-sub(ak=-akk,res)];
resc;
intgc:=2*ima*Pi*[sub(ak=akk,resc)-sub(ak=-akk,resc)];

T1:=sub(s=ss,amplg)-sub(s=-ss,amplgc);

→Amplitude
intg;
intgc;
amplg:=jac*ft*intg;
amplgc:=jac*ft*intgc;
amplg:=amplg/(2*akk);
amplgc:=amplgc/(2*akk);
let akk**2=x;
let kt.kt=ktt;
let la**2=l;

T2:=sub(s=ss,amplg)-sub(s=-ss,amplgc);

on factor;
amplg;
amplgc;
%Integration sur alpha: fichier avsac2.red
end;

```

```

→AMPL VERSUS AMPLGC
→Integration on alpha
intg:=((ima**6*ktt**6*x+ima**6*ktt**6+ima**6*1**6*s*x
-ima**6*1**6*s-2*ima**5*ktt**2*1**5-2*ima**5*1**5*s**2*x**2
+2*ima**5*1**5*s**2*x+ima**4*ktt**3*1**4+3*ima**4*ktt**2*1**4*s*x
-2*ima**4*ktt**2*1**4*s+ima**4*ktt**1**4*s**2*x**2-13*ima**4*ktt**1**4*s**2*x
+6*ima**4*ktt**1**4*s**2+ima**4*1**4*s**3*x**2-ima**4*1**4*s**3*x
+4*ima**3*ktt**3*1**3*s+16*ima**3*ktt**2*1**3*s**2*x-16*ima**3*ktt**2*1**3*s**2
+4*ima**3*ktt**1**3*s**3*x-ima**2*ktt**4*1**2*s-3*ima**2*ktt**3*1**2*s**2*x
+14*ima**2*ktt**3*1**2*s**2-ima**2*ktt**2*1**2*s**3*x**2-2*ima**2*ktt**2*1**2*s**3*x
+2*ima**2*ktt**1**2*s**4*x**2-2*ima**2*ktt**1**2*s**4*x-4*ima**ktt**4*1*s**2
-4*ima**ktt**2*1*s**4*x**2+4*ima**ktt**2*1*s**4*x-ktt**4*s**3*x
-2*ktt**3*s**4*x)*gs**4*ima**4*pi*s)
/((ima**2*1**2*x-ima**2*1**2+2*ima**ktt**1-ktt**2)**2*(ima**2*1**2-s**2*x)**2*1);
intgc:=(-(ima**6*ktt**6*x+ima**6*ktt**6-ima**6*1**6*s*x
+ima**6*1**6*s-2*ima**5*ktt**2*1**5-2*ima**5*1**5*s**2*x**2
+2*ima**5*1**5*s**2*x+ima**4*ktt**3*1**4-3*ima**4*ktt**2*1**4*s*x
+2*ima**4*ktt**2*1**4*s+ima**4*ktt**1**4*s**2*x**2-13*ima**4*ktt**1**4*s**2*x
+6*ima**4*ktt**1**4*s**2-ima**4*1**4*s**3*x**2+ima**4*1**4*s**3*x
-4*ima**3*ktt**3*1**3*s+16*ima**3*ktt**2*1**3*s**2*x-16*ima**3*ktt**2*1**3*s**2
-4*ima**3*ktt**1**3*s**3*x+ima**2*ktt**4*1**2*s-3*ima**2*ktt**3*1**2*s**2*x
+14*ima**2*ktt**3*1**2*s**2+ima**2*ktt**2*1**2*s**3*x**2+2*ima**2*ktt**2*1**2*s**3*x
+2*ima**2*ktt**1**2*s**4*x**2-2*ima**2*ktt**1**2*s**4*x-4*ima**ktt**4*1*s**2
-4*ima**ktt**2*1*s**4*x**2+4*ima**ktt**2*1*s**4*x+ktt**4*s**3*x
-2*ktt**3*s**4*x)*gs**4*ima**4*pi*s)/((ima**2*1**2*x
-ima**2*1**2+2*ima**ktt**1-ktt**2)**2*(ima**2*1**2-s**2*x)**2*1);
intg;
intgc;

T3:=sub(s=ss,intg)-sub(s=-ss,intgc);

inta;
intac;

T5:=sub(s=ss,inta)-sub(s=-ss,intac);

ao:=sub(x=0,inta);
aoc:=sub(x=0,intac);
x:=1/y;
inta;
intac;
let log((ima**2 *1**2 *y-s**2)/y)=log(ima**2 *1**2 *y-s**2)-log(y);
let log((-ima**2 *1**2 *y+ima**2 *1**2+2*ima**ktt**2 *1*y-kt**4*y)/y)
=log(-ima**2 *1**2 *y+ima**2 *1**2+2*ima**ktt**2 *1*y-kt**4*y)-log(y);
ai:=sub(y=0,inta);
aic:=sub(y=0,intac);
amplg:=ai-ao;
amplgc:=aic-aoc;

T7:=sub(s=ss,amplg)-sub(s=-ss,amplgc);

Amplgt:=amplg+amplgc;
→Leading term
Samplg:=lterm(num(amplg),s)/lterm(den(amplg),s);
Samplgc:=lterm(num(amplgc),s)/lterm(den(amplgc),s);
Samplgt:=lterm(num(amplgt),s)/lterm(den(amplgt),s);

T9:=sub(s=-ss,Samplg)-sub(s=ss,Samplgc);

→Leading-Log
Lsa:=lterm(num(Samplg),log(s))/lterm(den(Samplg),log(s));
Lsac:=lterm(num(Samplgc),log(s))/lterm(den(Samplgc),log(s));
Lsat:=lterm(num(Samplgt),log(s))/lterm(den(Samplgt),log(s));

T10:=sub(s=ss,Lsa)-sub(s=-ss,Lsac);

end;

```

Bibliography

- [1] J. D. Bjorken, *Phys. Rev. D* **47** (1993) 101.
- [2] D. E. Soper, Lectures given at Theoretical Advanced Study Institute in Elementary Particle Physics (TASI 2000): Flavor Physics for the Millenium, Boulder, Colorado, 4-30 Jun 2000. Published in *Boulder 2000, Flavor physics for the millennium* 267-316 arXiv:hep-ph/0011256.
- [3] V. Barone and E. Predazzi, *High-Energy Particle Diffraction*, Springer, 2002.
- [4] A. Donnachie and P. V. Landshoff, *Nucl. Phys. B* **244** (1984) 322.
- [5] G. Ingelman and P. E. Schlein, *Phys. Lett. B* **152** (1985) 256.
- [6] G. Ingelman, *Int. J. Mod. Phys. A* **21** (2006) 1805 [arXiv:hep-ph/0512146].
- [7] M. Arneodo and M. Diehl, arXiv:hep-ph/0511047, proceedings of HERA and the LHC: A Workshop on the Implications of HERA for LHC Physics: CERN - DESY Workshop 2004/2005 (Midterm Meeting, CERN, 11-13 October 2004;
- [8] J. R. Cudell and O. F. Hernandez, *Nucl. Phys. B* **471** (1996) 471 [arXiv:hep-ph/9511252].
- [9] D. Acosta *et al.* [CDF Collaboration], “Inclusive double pomeron exchange at the Fermilab Tevatron $\bar{p}p$ *Phys. Rev. Lett.* **93** (2004) 141601 [arXiv:hep-ex/0311023].
- [10] K. Goulianos, Presented at 11th International Conference on Elastic and Diffractive Scattering: Towards High Energy Frontiers: The 20th Anniversary of the Blois Workshops, Chateau de Blois, Blois, France, 15-20 May 2005. arXiv:hep-ph/0510035.
- [11] [TOTEM Collaboration], Letter of intend, CERN-LHCC-1997-049.
- [12] G. Anelli *et al.* [TOTEM Collaboration], arXiv:hep-ex/0602025.
- [13] A. Donnachie and P. V. Landshoff, *Phys. Lett. B* **296** (1992) 227 [arXiv:hep-ph/9209205].
- [14] J. R. Cudell, A. Lengyel and E. Martynov, *Phys. Rev. D* **73** (2006) 034008 [arXiv:hep-ph/0511073].
- [15] S. Abatzis *et al.* [WA91 Collaboration], *Phys. Lett. B* **324** (1994) 509.
- [16] E. A. Kuraev, L. N. Lipatov and V. S. Fadin, *Sov. Phys. JETP* **44** (1976) 443 [*Zh. Eksp. Teor. Fiz.* **71** (1976) 840].
- [17] I. I. Balitsky and L. N. Lipatov, *Sov. J. Nucl. Phys.* **28** (1978) 822 [*Yad. Fiz.* **28** (1978) 1597].
- [18] S. J. Brodsky, V. S. Fadin, V. T. Kim, L. N. Lipatov and G. B. Pivovarov, arXiv:hep-ph/0111390, SLAC-PUB-9069, CERN-TH-2001-341, Nov 2001.

- [19] J. R. Forshaw, Contributed to HERA and the LHC: A Workshop on the Implications of HERA and LHC Physics (Startup Meeting, CERN, 26-27 March 2004; Midterm Meeting, CERN, 11-13 October 2004), Hamburg, Germany, 21-24 Mar 2005. arXiv:hep-ph/0508274.
- [20] A. Bialas and P. V. Landshoff, Phys. Lett. B **256** (1991) 540.
- [21] M. Acciarri *et al.* [L3 Collaboration], Phys. Lett. B **461** (1999) 376 [arXiv:hep-ex/9909004].
- [22] P. V. Landshoff, Nucl. Phys. Proc. Suppl. **99A** (2001) 311 [arXiv:hep-ph/0010315].
- [23] A. D. Martin, V. A. Khoze and M. G. Ryskin, arXiv:hep-ph/0605189 and references.
- [24] V. A. Khoze, A. D. Martin and M. G. Ryskin, Eur. Phys. J. C **23** (2002) 311 [arXiv:hep-ph/0111078].
- [25] R. Enberg, G. Ingelman, A. Kissavos and N. Timneanu, Phys. Rev. Lett. **89** (2002) 081801 [arXiv:hep-ph/0203267].
- [26] V. A. Khoze, A. D. Martin and M. G. Ryskin, Eur. Phys. J. C **26** (2002) 229 [arXiv:hep-ph/0207313].
- [27] M. E. Peskin and D. V. Schroeder, *An Introduction to quantum field theory*, Westview Press, 1995.
- [28] F. Halzen and A. D. Martin, *Quarks And Leptons: An Introductory Course In Modern Particle Physics*, John Wiley, 1984.
- [29] R. Krönig, J. Op. Soc. Am., **12** (1926) 547; H. A. Kramers, Atti Congr. Intern. Fisici Como, (1927).
- [30] J. D. Bjorken and S. D. Drell, *Relativistic Quantum Field Theory*, McGraw-Hill Book Company, 1965.
- [31] J. D. Jackson, *Classical Electrodynamics*, Jhon Wiley & Sons, Second Edition, 1975.
- [32] R. E. Cutkosky, J. Math. Phys. **1** (1960) 429.
- [33] J. C. Collins, Pedagogical summary arXiv:hep-ph/9705393.
- [34] I. Y. Pomeranchuk, Sov. J. Nucl. Phys. JETP **3** (1956) 306.
- [35] J. R. Forshaw and D. A. Ross, *Quantum Chromodynamics and the Pomeron*, Cambridge University Press, 1997.
- [36] J. D. Bjorken, Nucl. Phys. Proc. Suppl. **25B** (1992) 253.
- [37] H. Cheng and T. T. Wu, *Expanding Protons: Scattering at High Energies*, MIT Press, 1987.
- [38] V. N. Gribov, Nucl. Phys. B **139** (1978) 1.
- [39] R. P. Feynman, Acta Phys. Polon. **24** (1963) 262.
- [40] B. S. DeWitt, Phys. Rev. **162** (1967) 1195.
- [41] L. D. Faddeev and V. N. Popov, Phys. Lett. B **25** (1967) 29.

-
- [42] J. R. Cudell, *A short course on Quantum Chromodynamics*, Gand, 2004, <http://qcd.theo.phys.ulg.ac.be/cudell/QCD/index.html>.
- [43] Y. L. Dokshitzer and D. E. Kharzeev, *Ann. Rev. Nucl. Part. Sci.* **54** (2004) 487 [arXiv:hep-ph/0404216].